

# Circuit-Noise-Resilient Virtual Distillation

Xiao-Yue Xu,<sup>1</sup> Chen Ding,<sup>1</sup> Shuo Zhang,<sup>1</sup> Wan-Su Bao,<sup>1,2,\*</sup> and He-Liang Huang<sup>1,2,†</sup>

<sup>1</sup>Henan Key Laboratory of Quantum Information and Cryptography, Zhengzhou, Henan 450000, China

<sup>2</sup>Hefei National Laboratory, University of Science and Technology of China, Hefei 230088, China

(Dated: November 15, 2023)

Quantum error mitigation (QEM) is crucial for near-term quantum devices, as noise inherently exists in physical quantum systems and undermines the accuracy of quantum algorithms. A typical purification-based QEM method, called Virtual Distillation (VD), aims to mitigate state preparation errors and achieve effective exponential suppression using multiple copies of the noisy state. However, imperfect VD circuit implementation may yield negative mitigation outcomes, potentially more severe than those achieved without QEM. To address this, we introduce Circuit-Noise-Resilient Virtual Distillation (CNR-VD). This method, featuring a calibration procedure that utilizes easily-prepared input states, refines the outcomes of VD when its circuit is contaminated by noise, seeking to recover the results of an ideally conducted VD circuit. Simulation results demonstrate that the CNR-VD estimator effectively reduces deviations induced by noise in the VD circuit, showcasing improvements in accuracy by an order of magnitude at most compared to the original VD. Meanwhile, CNR-VD elevates the gate noise threshold for VD, enabling positive effects even in the presence of higher noise levels. Furthermore, the strength of our work lies in its applicability beyond specific QEM algorithms, as the estimator can also be applied to generic Hadamard-Test circuits. The proposed CNR-VD significantly enhances the noise-resilience of VD, and thus is anticipated to elevate the performance of quantum algorithm implementations on near-term quantum devices.

*Introduction.*— In the pursuit of large-scale fault-tolerant quantum computers, the presence of noise arising from environmental noise and imperfect hardware remains a significant challenge. [1–4]. The field of Quantum error mitigation (QEM) techniques [5–14] braves this challenge, offering hopeful solutions that reduce the impact of noise even in the absence of full-blown quantum error correction [15–18]. Among these techniques, purification-based QEM methods [19–22] have gained considerable attention for their ability to mitigate errors without relying on specific noise assumptions. These methods aim to extract the ideal state from many copies of the noisy state. Virtual distillation (VD) [23–25] is a typical purification-based QEM algorithm. By utilizing  $n$  copies of an  $N$ -qubit noisy state which is contaminated by state preparation errors, the  $n$ -order VD has the distinguished ability to exponentially reduce errors in expectation value estimation for an observable  $O$ . This unique feature highlights the significance of VD in the field of QEM.

However, employing VD algorithm for high-accuracy expectation values encounters two primary challenges. The first challenge is the coherent mismatch [23, 24, 26], which can be mitigated through combinations of other QEM methods such as quantum subspace expansion [11, 27, 28] in the state preparation circuit [10], or polynomial fitting of multiple orders of VD [24]. The second challenge arises from noise in the VD circuit. The Hadamard-Test-like VD circuit [24], which can be utilized to efficiently implement VD, consists of controlled derangement operator  $D_n$  and controlled operator  $O$ . As the number of multi-qubit gates in the VD circuit increases linearly with  $nN$  [24], it can introduce non-negligible deviations in the estimated expectation values, potentially surpassing the initial errors in state preparation. Mitigating this error often

involves treating the VD circuit as a part of the target circuit and leveraging additional QEM techniques [24], or employing shadow estimations [29–31] to avoid executing the VD circuit, albeit with an exponential measurement overhead [22, 25].

In this work, we focus on mitigating the noise in the VD circuit and propose a novel approach called Circuit-Noise-Resilient Virtual Distillation (CNR-VD). In our method, we integrate a calibration procedure that utilizes the noisy VD circuit. During this procedure, the noisy state  $\rho$  undergoes a transformation into easily-prepared states that are independent of  $\rho$ . The expectation values of these states are obtained via noisy VD (VD with a noisy VD circuit), and are subsequently employed to enhance mitigation outcomes, which is facilitated by a function derived from noisy VD. Numerical results confirm the effectiveness of CNR-VD, demonstrating a significant improvement in accuracy—up to an order of magnitude—compared to noisy VD. We also observe that CNR-VD raises the gate noise threshold for VD, resulting in effective mitigation outcomes. Moreover, we compare the accuracy and efficiency of CNR-VD with two common VD-based methods designed to counter noise in the VD circuit, and observe the superiority of CNR-VD.

*Virtual distillation with noisy VD circuit.*— Suppose we have an  $N$ -qubit noisy quantum state  $\rho$ . Through spectral decomposition, the noisy state  $\rho$  can be expressed as  $\rho = (1 - \epsilon)|\psi\rangle\langle\psi| + \epsilon \sum_k \lambda_k |\psi_k\rangle\langle\psi_k|$  where  $\epsilon \geq 0$  is the error rate, along with the dominant eigenstate  $|\psi\rangle\langle\psi|$  and the noisy components  $\sum_k \lambda_k |\psi_k\rangle\langle\psi_k|$  (satisfying  $\sum_k \lambda_k = 1$ ) of  $\rho$ . The  $n$ -order VD algorithm is designed to distill  $|\psi\rangle\langle\psi|$  using  $n$  copies of  $\rho$ . For a  $k$ -weight ( $k \leq N$ ) Pauli observable  $O = \sum_{\omega=1}^k O^{i_\omega}$  where the  $\omega$ -th non-trivial Pauli term on qubit  $Q_{i_\omega}$  is  $O^{i_\omega} \in \{\sigma_x, \sigma_y, \sigma_z\}$ , the  $n$ -order mitigated expectation value obtained via VD is  $\langle O \rangle_{\text{VD}} = \frac{\text{Tr}[\rho^n O]}{\text{Tr}[\rho^n]} \approx \langle \psi | O | \psi \rangle + \mathcal{O}(\epsilon^n)$ . By means of the VD circuit, we do not require the physical preparation of  $\rho^n$ . The VD circuit consists of the controlled derangement operator  $D_n$  containing

\* bws@qiclab.cn

† quanhh1@ustc.edu.cn

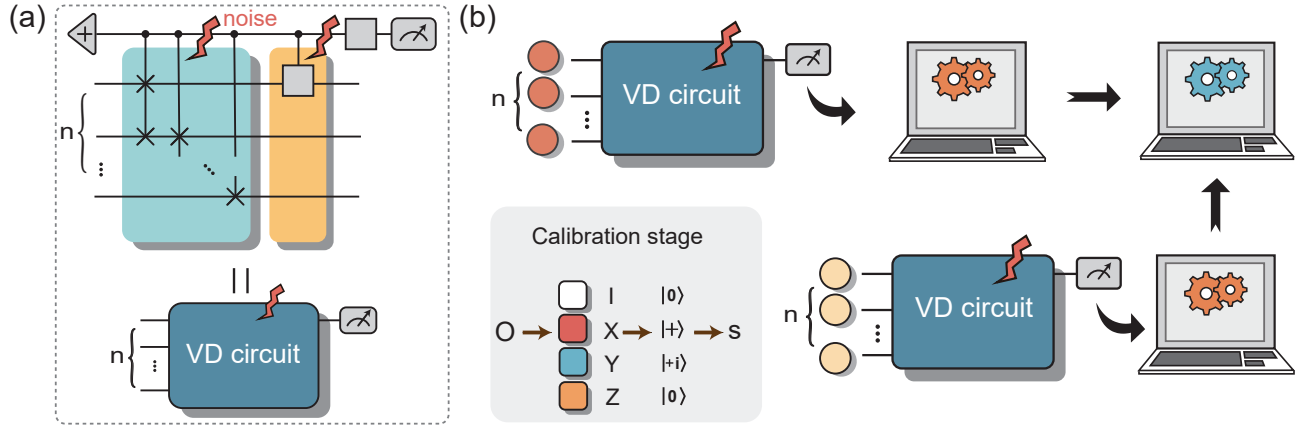


FIG. 1. **The noisy Virtual Distillation (VD) circuit and the circuit-noise-resilient virtual distillation (CNR-VD).** (a) The noisy VD circuit of  $n$ -order VD to estimate the expectation value of Pauli observable  $O$ , which consists of a noisy controlled derangement operator  $\tilde{D}_n$  and a controlled operator  $\tilde{O}$ . (b) The procedure of CNR-VD. In the  $n$ -order noisy VD (VD with noisy VD circuit), we use  $n$  copies of the noisy state  $\rho$  to compute the estimator  $\hat{O}_{\text{VD}}(\rho)$ . The CNR-VD estimator  $\hat{O}_{\text{CNR-VD}}(\rho)$  can be expressed as a function of  $\hat{O}_{\text{VD}}(\rho)$ , and the parameters of the function which can be some expectation value  $\hat{O}_{\text{VD}}(s)$  calculated by noisy VD with input state  $s$ . The parameters are obtained in the newly added calibration procedure. And the state  $s$  can be chosen to be the eigenstate of Pauli observable  $O$  with eigenvalue  $\pm 1$ , which is separate and easily-prepared. In the calibration procedure highlighted in the gray box in (b), we show one possible choice for  $s$  which is the eigenstate of Pauli  $O$  with eigenvalue  $+1$ .

$nN$  CSWAP gates, and the controlled Pauli operator  $O$  consisting of  $k$  two-qubit controlled Pauli gates. Accordingly, the mitigated value gives as

$$\langle O \rangle_{\text{VD}} = \frac{\text{Tr}[\rho^n O]}{\text{Tr}[\rho^n]} = \frac{\text{Tr}[D_n((\rho O) \otimes \rho^{\otimes n-1})]}{\text{Tr}[D_n \rho^{\otimes n}]}, \quad (1)$$

where  $\text{Tr}[\rho^n O]$  is calculated by  $2p_0(\rho, O) - 1$  with the probability  $p_0(\rho, O)$  of measuring the ancilla qubit  $Q_0$  in the zero state. We can use the same way to estimate  $\text{Tr}[\rho^n]$  by replacing  $O$  with  $I$  in the VD circuit.

Given that multi-qubit gate noise is the primary noise source in the VD circuit, for the sake of simplicity, we primarily concentrate on addressing the effects of the multi-qubit gate noise. We assume the  $m$ -qubit ( $m \geq 2$ ) stochastic Pauli gate noise  $\mathcal{E}_m^p(\rho) = (1 - p_m)\rho + p_m \sum_{s=1}^{4^m-1} \delta_s^m P_s^m \rho P_s^m$  for multi-qubit gates, where  $p_m \geq 0$  is the Pauli error rate and the coefficients  $\{\delta_s^m\}_s$  of the  $m$ -qubit Pauli error terms  $\{P_s^m\}_s$  satisfies  $\delta_s^m \geq 0, \sum_s \delta_s^m = 1$ . Considering that measurement error mitigation protocols [32–38] such as Tensor Product Noise (TPN) [35, 39] can effectively suppress single-qubit readout errors in VD, which purely involves measurements on one qubit, we set up clean readout of the ancilla. We denote  $\tilde{p}_0(\rho, O)$  as the noisy version of  $p_0(\rho, O)$  which is contaminated by the noise in the VD circuit, and we will pay our attention to the second-order VD under the Pauli gate noise assumption. Then the outcome gained through noisy VD circuit can be expressed as a function

$$2\tilde{p}_0(\rho, O) - 1 = \sum_{j=0}^{\lfloor \frac{k}{2} \rfloor} \sum_{t=0}^{\binom{k}{j}-1} a_{j,t}^k(p_2, p_3, O) A_j(t), \quad (2)$$

where  $j$  denotes the number of unwanted SWAP gates generated by  $\sigma_x/\sigma_y$  Pauli errors occurring on the controlled qubit

of CSWAP gates, and  $t$  represents the  $t$ -th combination of positions for these  $j$  SWAPs. And  $a_{j,t}^k(p_2, p_3, O)$  refers to the  $\rho$ -independent parameters for  $A_j(t)$  (we define  $A_0(0) = A_k(0) = \text{Tr}[\rho^2 O]$ ) which can be written as

$$A_j(t) = (1 - \epsilon)^2 \text{Tr}[O_1^{j,t} |\psi\rangle\langle\psi|] \cdot \text{Tr}[O_2^{j,t} |\psi\rangle\langle\psi|] + \epsilon^2 \sum_k \lambda_k^2 \text{Tr}[O_1^{j,t} |\psi_k\rangle\langle\psi_k|] \cdot \text{Tr}[O_2^{j,t} |\psi_k\rangle\langle\psi_k|]. \quad (3)$$

$A_j(t)$  is a combination of expectation values of observables  $O_1^{j,t}$  and  $O_2^{j,t}$  which meets  $O = O_1^{j,t} + O_2^{j,t}$ , and it derives from the  $t$ -th combination of  $j$  undesired SWAPs (See more details in the SM).

*Circuit-Noise-Resilient virtual distillation.*— Now we will introduce the CNR-VD, which aims to extract  $\text{Tr}[\rho^2 O]$  attained by ideal VD (VD with noiseless VD circuit) based on the function in Eq. 2. We begin with the simplest case involving a one-weight Pauli observable  $O$  (equally applicable to  $I$ ), which holds  $A_j(t) = \text{Tr}[\rho^2 O]$  for  $j = 0, 1$  and  $t = 0$ . Then Eq. 2 reduces to

$$2\tilde{p}_0(\rho, O) - 1 = a(p_2, p_3, O) \text{Tr}[\rho^2 O]. \quad (4)$$

The  $\rho$ -independent parameter  $a(p_2, p_3, O)$  is amenable to calibrate if we assume the temporal stability of Pauli error rate  $p_3(p_2)$ . In order to obtain these parameters, we add a calibration procedure using the noisy VD circuit where the noisy state  $\rho$  is replaced by some easily-prepared state  $s$ , as showed in the Fig. 1(b). The state  $s$  can be any eigenstate of  $O$  with eigenvalue  $+1$  which satisfies  $\text{Tr}[s^2 O] = 1$ , and the parameter  $a(p_2, p_3, O)$  in Eq. 4 can be calculated by  $2\tilde{p}_0(s, O) - 1$ . We can also attain the parameter  $a(p_2, p_3, I)$  for  $\text{Tr}[\rho^2]$  through noisy VD circuit with  $O = I$ . Then with the noisy VD estimator defined as  $\hat{O}_{\text{VD}}(\rho) = (2\tilde{p}_0(\rho, O) - 1)/(2\tilde{p}_0(\rho, I) - 1)$ ,

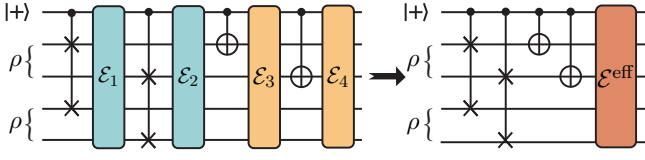


FIG. 2. **The effective noise of the second-order VD circuit.** For the two-qubit noisy state  $\rho$  and two-weight Pauli observable  $\sigma_x^{\otimes 2}$ , there are four layers of gates containing two CSWAP gates and two CX gates in total. We define the general global Markovian noise of the  $i$ -th layer as  $\mathcal{E}_{i+1}$ . After relocating all the noise to the end of the VD circuit, we define the mixture of these noise conjugated by the layers behind as the effective noise  $\mathcal{E}^{\text{eff}}$ .

we can establish the CNR-VD estimator

$$\hat{O}_{\text{CNR-VD}}(\rho) = \frac{\left(\frac{2\tilde{p}_0(\rho, O) - 1}{2\tilde{p}_0(s, O) - 1}\right)}{\left(\frac{2\tilde{p}_0(\rho, I) - 1}{2\tilde{p}_0(s, I) - 1}\right)} = \frac{\hat{O}_{\text{VD}}(\rho)}{\hat{O}_{\text{VD}}(s)}, \quad (5)$$

which exhibits full resilience to the noise in the VD circuit for any one-weight Pauli observable  $O$ . We can also employ the CNR-VD estimator to obtain reliable expectation values for higher-weight Pauli observables under moderate noise level of Pauli gate noise, with an estimation error  $\mathcal{O}(p_2, p_3)$  as we ignore terms in Eq. 2 with  $j > 1$ . When the assumption of stochastic Pauli gate noise model in our work does not suit the practical scenario, the employment of randomized compiling [40–42] (RC) technique can enable us come close to the stochastic Pauli gate noise. Since the CSWAPs in the VD circuit are not Clifford, we choose a small Pauli subgroup as the twirling set for CSWAPs and demonstrate its effectiveness through numerical simulations (See details of implementation RC in the SM). Moreover, since the independence on  $\rho$  of the parameters in Eq. 4, it is more efficient to estimate several noisy states and observables while executing the calibration procedure only once to minimize the circuit resource consumption, as long as the temporal stability of gate noise holds at least during a certain time period.

Besides the local Pauli gate noise model, our CNR-VD estimator is also applicable to the general Markovian noise model without restrictions on locality. For the  $n$ -order VD, in order to directly express how the noise in the VD circuit contributes to  $\tilde{p}_0(\rho, O)$ , we propagate all the noise in the VD circuit backward to the end of the circuit. Suppose the VD circuit has  $l$  layers of noisy gates  $\tilde{U}_{1:l} = \prod_{j=1}^l \mathcal{E}^j \mathcal{U}_j$ , where  $\mathcal{E}^j$  is the Markovian noise acting on the  $j$ -th layer. Then the  $j$ -th noise  $\mathcal{E}^j$  will be conjugated by all the ideal gates  $\mathcal{U}_{j+1:l}$  subsequent to  $\mathcal{U}_j$  and it turns to  $\mathcal{U}_{j+1:l}^\dagger \mathcal{E}^j \mathcal{U}_{j+1:l}$  when relocated to the end. We define the  $(nN + 1)$ -qubit mixture of these conjugated noise as the effective noise  $\mathcal{E}^{\text{eff}}(\cdot) = \sum_i K_i \cdot K_i^\dagger$  of the VD circuit, where  $K_i$  is the Kraus operator of the effective noise. Hence, the noisy VD circuit can be divided into an ideal VD circuit followed by the effective noise, as shown in Fig 2. We define an  $(nN + 1)$ -qubit state  $\rho^{\text{RD}} = \rho^{\text{R}} \otimes \rho^{\text{D}}$  where  $\rho^{\text{R}}$  is a single-qubit pure state and  $\rho^{\text{D}}$  is an  $(nN)$ -qubit operator. Then if the effective noise  $\mathcal{E}^{\text{eff}}$  satisfies any of these two conditions:

- There exists a set of Kraus operators such that: each

Kraus operator  $K_i = K_i^{\text{R}} \otimes K_i^{\text{D}}$  of  $\mathcal{E}^{\text{eff}}$  is separate into subsystems  $\rho^{\text{R}}$  and  $\rho^{\text{D}}$ , along with unitary  $K_i^{\text{R}}$  and  $K_i^{\text{D}}$ .

- $\mathcal{E}^{\text{eff}} = \mathcal{E}^{\text{eff,R}} \otimes \mathcal{E}^{\text{eff,D}}$ , along with the single-qubit unital noise channel  $\mathcal{E}^{\text{eff,R}}$  and the CPTP noise channel  $\mathcal{E}^{\text{eff,D}}$ ,

the CNR-VD estimator  $\hat{O}_{\text{CNR-VD}}(\rho)$  can reduce the error in the expectation value induced by  $\mathcal{E}^{\text{eff}}$  (See proofs in the SM). Since the depolarizing gate noise satisfies Condition 2 as it commutes with the CSWAP gates in the VD circuit,  $\hat{O}_{\text{CNR-VD}}(\rho)$  show high tolerance to low-error-rate Pauli gate noise which is close to the depolarizing gate noise. We also establish other form of the CNR-VD estimator with loosen requirement of  $\mathcal{E}^{\text{eff}}$  in the SM.

Furthermore, we can extend our CNR-VD to encompass a broader range of quantum computing applications beyond QEM algorithms. By generalizing the operators  $D_n$  and  $O$  in the VD circuit to arbitrary Hermitian operator  $U$ , we can get a typical Hadamard-Test circuit. Then we can use the CNR-VD estimator to calculate the expectation value of  $\text{Tr}[\rho U]$  and reduce the additional noise caused by the controlled- $U$ . As for the input state  $s$  used in the calibration procedure, we can choose any state that satisfies  $\text{Tr}[sU] = 1$  (See more details and simulations in the SM).

*Numerical simulations.*—To evaluate the performance of CNR-VD, we conduct various numerical simulations and compare its results among those obtained from noisy VD and other VD-based methods. To quantify the accuracy of estimators we use the absolute error between the ideal and estimated expectation values of observable  $O$ , calculated as  $\text{Error} = |\langle O \rangle^{\text{est}} - \langle O \rangle^{\text{ideal}}|$ . For a fair comparison, we configure the same total measurement shot number for each method. We utilize second-order VD and perform the calibration procedure in each independent repeated experiment.

Our investigation begins with ascertaining the accuracy of CNR-VD with fluctuating weights of observables, noise levels of the VD circuit, and state preparation error rates. The stochastic Pauli gate noise model is utilized eliminating the need for RC technique. We denote the average error rate of two-qubit gates as the noise level of the VD circuit and then set corresponding Pauli error rates  $p_2$  and  $p_3$  (See the detailed settings in the SM). We generate random noisy state  $\rho_r = (1-\epsilon)|\psi\rangle\langle\psi| + \epsilon|\psi_e\rangle\langle\psi_e|$  with the state preparation error rate  $\epsilon$  by randomly choosing pure state  $|\psi\rangle\langle\psi|$  and  $|\psi_e\rangle\langle\psi_e|$  which are mutually orthogonal. As the target noiseless state  $|\psi\rangle\langle\psi|$  is exactly the dominant eigenstate of  $\rho_r$ , our results using VD-based methods are free from coherent mismatch.

We first carry out simulations of 4-qubit random states with a fixed state preparation error rate 0.10, in comparison with ideal VD and noisy VD as illustrated in Fig. 3(a). The noise level ranges from  $10^{-4}$  to  $10^{-1}$ , and the Pauli observables are randomly assigned with weight 1 and 4. Results demonstrate that CNR-VD well recovers the outcomes obtained by ideal VD for low-weight observables or moderate noise levels. Our subsequent focus lays in the noise threshold at which the error-mitigated methods provide enhanced results compared to unmitigated estimation. With reference to the diagram in Fig. 3(b), we annotate the inflection points where noisy VD and CNR-VD start to perform worse than unmitigated estima-

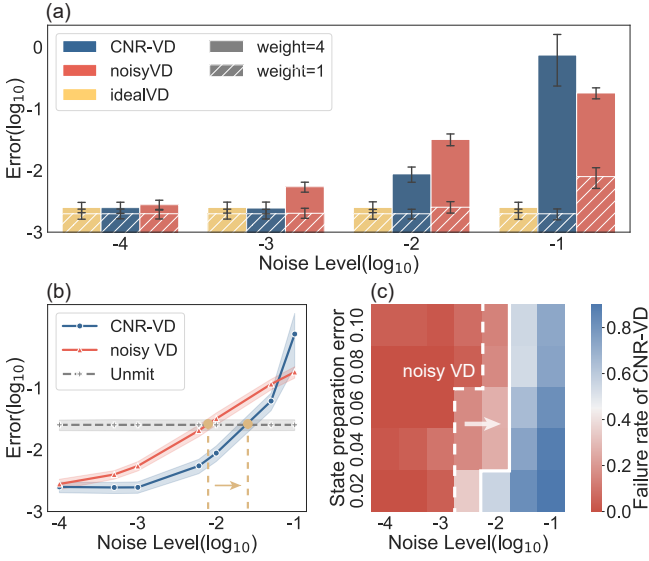


**FIG. 3. The accuracy of CNR-VD under Pauli gate noise with varying weights of observables, noise levels of the VD circuit and state preparation error rates.** (a) Results of 4-qubit random states under state preparation error rate 0.10 obtained from CNR-VD, ideal VD (VD with noiseless VD circuit) and noisy VD (VD with noisy VD circuit) with increasing noise levels of the VD circuit from  $10^{-4}$  to  $10^{-1}$  and random Pauli observables of weight 1 and 4. (b) Accuracy of 4-qubit random states under state preparation error rate 0.10 shifting with an increase in the noise level, in comparison with noisy VD and unmitigated estimation (Unmit). To identify the noise threshold at which the VD-based estimators can achieve improved results compared to unmitigated estimation, we mark the inflection points with yellow dots and indicate the corresponding noise level thresholds with yellow dashed lines. (c) Failure rate of CNR-VD with changing noise levels and state preparation error rates. The failure rate represents the probability that CNR-VD produces results inferior to the unmitigated estimation. A boundary at 0.5 failure rate of CNR-VD is marked by a white solid line, indicating the point at which the resilience to noise of CNR-VD depletes. Additionally, the corresponding failure rate boundary for noisy VD is represented by a white dashed line. The displayed data represents the average outcome derived from 50 separate experiments with different random states.

tion using yellow dots and indicate the corresponding noise thresholds with dashed lines. The increased noise threshold highlights the superiority of CNR-VD over noisy VD. In addition, we evaluate the failure rate of CNR-VD contingent on fluctuating noise levels and state preparation error rates. The failure rate signifies the probability that the results generated by CNR-VD are inferior to unmitigated estimation. Since the accuracy of unmitigated estimation is merely determined by the state preparation error, larger state preparation error rate relatively to the noise level of the VD circuit tends to result in smaller failure rate, in accordance with the data shown in Fig. 3(c). A boundary at failure rate 0.5 for CNR-VD is marked by a solid white line, signalling the point where CNR-VD's resilience to noise diminishes. The corresponding failure rate boundary for the noisy VD is also highlighted by a white dashed line. From our observations, CNR-VD extends

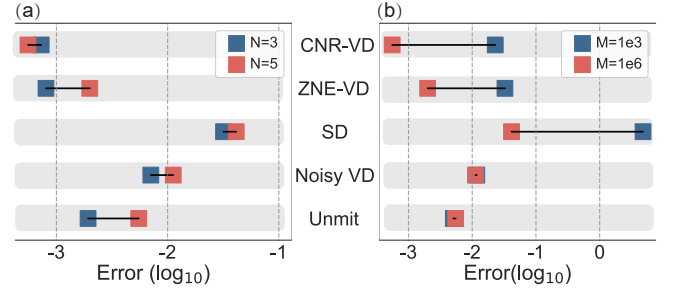


**FIG. 4. Comparison results of the expectation values of GHZ states obtained from several VD-based mitigation methods, with changing number of qubits  $N$  and total shots number  $M$ .** (a) Performance of five estimators: CNR-VD, ZNE-VD, SD, noisy VD and unmitigated estimation (Unmit) with fixed total shots number  $M = 10^6$ , and number of qubits 3 and 5. We employ RC with 4 random instance for both ZNE-VD and CNR-VD. (b) Performance of estimators for 5-qubit GHZ state, with total shots number  $10^3$  and  $10^6$ .

the boundary to higher noise level by up to one order of magnitude, which provides vital insights into the effectiveness and robustness of CNR-VD.

We also conduct a comparative study between CNR-VD and two common VD-based methods designed against noise in the VD circuit, which are Shadow Distillation [29] (SD) and noisy VD combined with zero-noise extrapolation (ZNE-VD) [24]. SD is a variation of VD that leverages shadow estimation to approximate the nonlinear function  $\text{Tr}[\rho^2 O]/\text{Tr}[\rho^2]$  of  $\rho$ . And ZNE-VD employs the zero-noise extrapolation (ZNE) [7, 13, 43–48] error mitigation scheme to mitigate the noise in the VD circuit. We configure the composite gate noise of depolarizing, phase damping and amplitude damping, and the noise level is set to be the error rate of each type of noise. (See the detailed settings in the SM). For both CNR-VD and ZNE-VD, we employ RC technique with 4 random instances in the VD circuit to enhance the effectiveness of the estimators. The comparisons involve the  $N$ -qubit GHZ state with the Pauli observable  $\sigma_x^{\otimes N}$ . We assess the accuracy across a range of qubit numbers, from 3 to 5, and for total measurement shot numbers  $M$  varying from  $10^3$  to  $10^6$ . We specifically illustrate the accuracy when using the maximum and minimum values of  $N$  or  $M$  to better demonstrate the trend. Results are given in Fig. 4.

We can observe that the accuracy of noisy VD exhibits an inferior performance compared to unmitigated estimation. This can be attributed to smaller state preparation error compared to the noise in the VD circuit, as the state preparation circuit for GHZ state only has  $N - 1$  noisy two-qubit CX gates while there are  $3N$  noisy multi-qubit gates in the VD circuit. However, CNR-VD remains its superiority in terms of accuracy even as the number of qubits increases. Notably, CNR-VD achieves an improvement in accuracy compared to noisy VD by more than an order of magnitude for 5-qubit GHZ state, as given in Fig. 4(a). And in Fig. 4(b), we can see that with the increasing number of shots, the performance of three VD-based methods (CNR-VD, ZNE-VD, SD) achieve significant enhancement in accuracy while the accuracy of noisy VD and



unmitigated estimation are unable to further improve. This also indicates that there are additional sampling overhead besides VD introduced by these methods to achieve improved accuracy. It is noteworthy that among the three VD-based methods, CNR-VD consistently maintains a clear advantage. Furthermore, simulation results of CNR-VD for higher order VD are provided in the SM, where CNR-VD exhibits the ability to recover the ideal behavior of 3-order VD with noise level lower than  $10^{-3}$ .

*Conclusion.*— In conclusion, we propose the CNR-VD estimator based on the VD error mitigation method. The CNR-VD estimator is established based on the original noisy VD and it effectively overcomes the potential harmful influence of gate noise in the VD circuit, without additional quantum resources such as qubits and gates. The simulation results demonstrate that our proposed method can achieve better mitigation performance under diverse noisy conditions, in comparison to noisy VD and other VD-based methods designed against noise in the VD circuit. Combined with randomized compiling technique we can conquer the impact of composite

gate noise and increase the threshold for noise level at which QEM algorithms outperform unmitigated estimations.

Moverover, since our theoretical analysis is not limited to the VD algorithm, the CNR-VD estimator can also provide an effective solution to the practical challenge of circuit noise for the Hadamard-Test algorithms. This opens up vast research opportunities for our future work, such as exploring advanced techniques of CNR-VD in more complex error environments, and investigating the practical implementation of our approach on real quantum computing platforms. We are confident that this study will bring new insights to the field of QEM and guide the next phase of research.

## ACKNOWLEDGMENTS

H.-L. H. acknowledges support from the Youth Talent Lifting Project (Grant No. 2020-JCJQ-QT-030), National Natural Science Foundation of China (Grant No. 12274464).

- 
- [1] J. Preskill, *Quantum* **2**, 79 (2018).
- [2] F. Arute, K. Arya, R. Babbush, D. Bacon, J. C. Bardin, R. Barends, R. Biswas, S. Boixo, F. G. S. L. Brandao, D. A. Buell, B. Burkett, Y. Chen, Z. Chen, B. Chiaro, R. Collins, W. Courtney, A. Dunsworth, E. Farhi, B. Foxen, A. Fowler, C. Gidney, M. Giustina, R. Graff, K. Guerin, S. Habegger, M. P. Harrigan, M. J. Hartmann, M. Ho, Alanand Hoffmann, T. Huang, T. S. Humble, S. V. Isakov, E. Jeffrey, Z. Jiang, D. Kafri, K. Kechedzhi, J. Kelly, P. V. Klimov, S. Knysh, A. Korotkov, F. Kostritsa, D. Landhuis, M. Lindmark, E. Lucero, D. Lyakh, J. R. Mandrà, Salvatoreand McClean, M. McEwen, A. Megrant, X. Mi, K. Michielsen, M. Mohseni, J. Mutus, O. Naaman, M. Neeley, C. Neill, M. Y. Niu, E. Ostby, A. Petukhov, J. C. Platt, C. Quintana, E. G. Rieffel, P. Roushan, N. C. Rubin, D. Sank, K. J. Satzinger, V. Smelyanskiy, K. J. Sung, M. D. Trevithick, A. Vainsencher, B. Villalonga, T. White, Z. J. Yao, P. Yeh, A. Zalcman, H. Neven, and J. M. Martinis, *Nature* **574**, 505 (2019).
- [3] H.-L. Huang, D. Wu, D. Fan, and X. Zhu, *Sci. China Inf. Sci.* **63**, 180501 (2020).
- [4] C. Ding, X.-Y. Xu, S. Zhang, H.-L. Huang, and W.-S. Bao, *Phys. Rev. A* **106**, 042421 (2022).
- [5] S. Endo, Z. Cai, S. C. Benjamin, and X. Yuan, *J. Phys. Soc. Japan* **90**, 032001 (2021).
- [6] A. Kandala, K. Temme, A. D. Córcoles, A. Mezzacapo, J. M. Chow, and J. M. Gambetta, *Nature* **567**, 491 (2019).
- [7] Y. Li and S. C. Benjamin, *Phys. Rev. X* **7**, 021050 (2017).
- [8] H.-L. Huang, X.-Y. Xu, C. Guo, G. Tian, S.-J. Wei, X. Sun, W.-S. Bao, and G.-L. Long, *Sci. China Phys. Mech. Astron.* **66**, 250302 (2023).
- [9] D. Qin, Y. Chen, and Y. Li, *Npj Quantum Inf.* **9**, 35 (2023).
- [10] N. Yoshioka, H. Hakoshima, Y. Matsuzaki, Y. Tokunaga, Y. Suzuki, and S. Endo, *Phys. Rev. Lett.* **129**, 020502 (2022).
- [11] S. McArdle, X. Yuan, and S. Benjamin, *Phys. Rev. Lett.* **122**, 180501 (2019).
- [12] S. McArdle, X. Yuan, and S. Benjamin, *Phys. Rev. Lett.* **122**, 180501 (2019).
- [13] Z. Cai, *Npj Quantum Inf.* **7**, 80 (2021).
- [14] C. Ding, X.-Y. Xu, Y.-F. Niu, S. Zhang, W.-S. Bao, and H.-L. Huang, *Sci. China Phys. Mech. Astron.* **66**, 230311 (2023).
- [15] J. Chiaverini, D. Leibfried, T. Schaetz, M. D. Barrett, R. B. Blakestad, J. Britton, W. M. Itano, J. D. Jost, E. Knill, C. Langer, R. Ozeri, and D. J. Wineland, *Nature* **432**, 602 (2004).
- [16] E. Knill, R. Laflamme, and L. Viola, *Phys. Rev. Lett.* **84**, 2525 (2000).
- [17] D. G. Cory, M. D. Price, W. Maas, E. Knill, R. Laflamme, W. H. Zurek, T. F. Havel, and S. S. Somaroo, *Phys. Rev. Lett.* **81**, 2152 (1998).
- [18] B. M. Terhal, *Rev. Mod. Phys.* **87**, 307 (2015).
- [19] M. Huo and Y. Li, *Phys. Rev. A* **105**, 022427 (2022).
- [20] Z. Cai, Resource-efficient purification-based quantum error mitigation (2021), [arXiv:2107.07279](https://arxiv.org/abs/2107.07279).
- [21] Y. Xiong, S. X. Ng, and L. Hanzo, *IEEE Trans. Commun.* **70**, 1927 (2022).
- [22] H.-Y. Hu, R. LaRose, Y.-Z. You, E. Rieffel, and Z. Wang, Logical shadow tomography: Efficient estimation of error-mitigated observables (2022), [arXiv:2203.07263](https://arxiv.org/abs/2203.07263).
- [23] W. J. Huggins, S. McArdle, T. E. O’Brien, J. Lee, N. C. Rubin, S. Boixo, K. B. Whaley, R. Babbush, and J. R. McClean, *Phys. Rev. X* **11**, 041036 (2021).
- [24] B. Koczor, *Phys. Rev. X* **11**, 031057 (2021).
- [25] A. Seif, Z.-P. Cian, S. Zhou, S. Chen, and L. Jiang, *PRX Quantum* **4**, 010303 (2023).
- [26] B. Koczor, *New J. Phys.* **23**, 123047 (2021).
- [27] J. I. Colless, V. V. Ramasesh, D. Dahlen, M. S. Blok, M. E. Kimchi-Schwartz, J. R. McClean, J. Carter, W. A. de Jong, and I. Siddiqi, *Phys. Rev. X* **8**, 011021 (2018).
- [28] J. Li, X. Yang, X. Peng, and C.-P. Sun, *Physical review letters* **118**, 150503 (2017).
- [29] R. Huang, Hsin-Yuanand Kueng and J. Preskill, *Nat. Phys.* **16**, 1050 (2020).
- [30] H.-Y. Huang, R. Kueng, and J. Preskill, *Phys. Rev. Lett.* **127**, 030503 (2021).
- [31] A. Elben, R. Kueng, H.-Y. R. Huang, R. van Bijnen, C. Kokail, M. Dalmonte, P. Calabrese, B. Kraus, J. Preskill, P. Zoller, and

- B. Vermersch, *Phys. Rev. Lett.* **125**, 200501 (2020).
- [32] F. B. Maciejewski, F. Baccari, Z. Zimborás, and M. Oszmaniec, *Quantum* **5**, 464 (2021).
- [33] H. Kwon and J. Bae, *IEEE Trans. Comput.* **70**, 1401 (2021).
- [34] Y. Chen, M. Farahzad, S. Yoo, and T.-C. Wei, *Phys. Rev. A* **100**, 052315 (2019).
- [35] S. Bravyi, S. Sheldon, A. Kandala, D. C. McKay, and J. M. Gambetta, *Phys. Rev. A* **103**, 042605 (2021).
- [36] F. B. Maciejewski, Z. Zimborás, and M. Oszmaniec, *Quantum* **4**, 257 (2020).
- [37] P. D. Nation, H. Kang, N. Sundaresan, and J. M. Gambetta, *PRX Quantum* **2**, 040326 (2021).
- [38] A. W. R. Smith, K. E. Khosla, C. N. Self, and M. S. Kim, *Sci. Adv.* **7**, eabi8009 (2021).
- [39] M. R. Geller, *Quantum Sci. Technol.* **5**, 03LT01 (2020).
- [40] J. J. Wallman and J. Emerson, *Phys. Rev. A* **94**, 052325 (2016).
- [41] A. Erhard, J. J. Wallman, L. Postler, M. Meth, R. Stricker, E. A. Martinez, P. Schindler, T. Monz, J. Emerson, and R. Blatt, *Nat. Commun.* **10**, 5347 (2019).
- [42] A. Hashim, R. K. Naik, A. Morvan, J.-L. Ville, B. Mitchell, J. M. Kreikebaum, M. Davis, E. Smith, C. Iancu, K. P. O'Brien, I. Hincks, J. J. Wallman, J. Emerson, and I. Siddiqi, *Phys. Rev. X* **11**, 041039 (2021).
- [43] S. Endo, S. C. Benjamin, and Y. Li, *Phys. Rev. X* **8**, 031027 (2018).
- [44] K. Temme, S. Bravyi, and J. M. Gambetta, *Phys. Rev. Lett.* **119**, 180509 (2017).
- [45] K. E. Hamilton and R. C. Pooser, *Quantum Mach. Intell.* **2**, 10 (2020).
- [46] A. Lowe, M. H. Gordon, P. Czarnik, A. Arrasmith, P. J. Coles, and L. Cincio, *Phys. Rev. Res.* **3**, 033098 (2021).
- [47] J. W. O. Garmon, R. C. Pooser, and E. F. Dumitrescu, *Phys. Rev. A* **101**, 042308 (2020).
- [48] S. Ferracin, A. Hashim, J.-L. Ville, R. Naik, A. Carignan-Dugas, H. Qassim, A. Morvan, D. I. Santiago, I. Siddiqi, and J. J. Wallman, Efficiently improving the performance of noisy quantum computers (2022), [arXiv:2201.10672](https://arxiv.org/abs/2201.10672).

# Supplemental Material for “Circuit-Noise-Resilient Virtual Distillation”

## VIRTUAL DISTILLATION

For an  $N$ -qubit noisy state  $\rho$ , the complete spectral decomposition of it can be expressed as

$$\rho = (1 - \epsilon)|\psi\rangle\langle\psi| + \epsilon \sum_k \lambda |\psi_k\rangle\langle\psi_k|, \quad (\text{S1})$$

where  $0 < \epsilon < 1$  is the state preparation error rate and  $|\psi\rangle\langle\psi|$  is the dominant eigenstate of  $\rho$ , along with the summation  $\sum_k$  which satisfies  $\sum_k \lambda_k = 1$  taking over all the noisy components of  $\rho$ . Given  $n$  identical copies of  $\rho$ , the error-mitigated expectation value of the Pauli observable  $O$  via virtual distillation (VD) is

$$\langle O \rangle_{\text{VD}} = \frac{\text{Tr}[\rho^n O]}{\text{Tr}[\rho^n]} = \frac{(1 - \epsilon)^n \langle \psi | O | \psi \rangle + \epsilon^n \sum_k \lambda_k^n \langle \psi_k | O | \psi_k \rangle}{(1 - \epsilon)^n + \epsilon^n \sum_k \lambda_k^n} = \langle \psi | O | \psi \rangle + \mathcal{O}(\epsilon^n), \quad (\text{S2})$$

which indicates that the approximation error  $\mathcal{O}(\epsilon^n)$  decays exponentially with the number of copies  $n$ . To efficiently estimate  $\text{Tr}[\rho^n O]$  ( $\text{Tr}[\rho^n]$ ), we utilize the VD circuit which consists of the controlled derangement operator  $D_n$  and the controlled operator  $O$ . The  $n$ -order VD circuit involves a three-qubit CSWAP gate chain  $\prod_{t=0}^{n-1} \prod_{i=0}^{N-1} \text{CSWAP}_{i,t}$  where  $\text{CSWAP}_{i,t}$  acts on qubit  $Q_0$ ,  $Q_{i+1+tN}$  and  $Q_{i+1+(t+1)N}$ , and a sequence of two-qubit controlled Pauli gates  $\prod_{j=1}^k \text{CO}_{i_j}$  where  $\text{CO}_{i_j}$  is applied on qubit  $Q_0$  and  $Q_{i_j+1}$ . And we denote the set of index of qubits on the nontrivial Pauli terms of the  $k$ -weight Pauli observable  $O$  as  $\mathcal{I}_k$ .

We denote the probability of measuring the ancilla qubit  $Q_0$  in the zero state as  $p_0(\rho, O)$  and the  $\text{Tr}[\rho^n O]$  can be estimated by  $2p_0(\rho, O) - 1$ . Take the second-order VD ( $n = 2$ ) for example, due to the linear properties of quantum computing, we can rewrite the probability  $p_0(\rho, O)$  according to the spectral decomposition

$$p_0(\rho, O) = (1 - \epsilon)^2 p_0(|\psi\rangle^{\otimes 2}, O) + 2\epsilon(1 - \epsilon) \sum_k \lambda_k p_0(|\psi\rangle|\psi_k\rangle, O) + \epsilon^2 \sum_{k,k'} \lambda_k \lambda_{k'} p_0(|\psi_k\rangle|\psi_{k'}\rangle, O). \quad (\text{S3})$$

In this way, we can focus on probability of the pure state in form of  $p_0(|\psi_a\rangle|\psi_b\rangle, O)$ . The input state of the VD circuit is  $|+\rangle|\psi_a\rangle|\psi_b\rangle$ , and we can obtain the final  $(2N + 1)$ -qubit density matrix  $\rho^{\text{out}}$  just before measurement by

$$\begin{aligned} \rho^{\text{fin}} = & \frac{1}{2} (|+\rangle|\psi_a\rangle|\psi_b\rangle\langle +| \langle \psi_a | \langle \psi_b | + |-\rangle O |\psi_b\rangle |\psi_a\rangle \langle -| \langle \psi_b | O \langle \psi_a | + \\ & |+\rangle|\psi_a\rangle|\psi_b\rangle \langle -| \langle \psi_b | O \langle \psi_a | + |-\rangle O |\psi_b\rangle |\psi_a\rangle \langle +| \langle \psi_a | \langle \psi_b |). \end{aligned} \quad (\text{S4})$$

Then we calculate the probability  $p_0(|\psi_a\rangle|\psi_b\rangle, O)$  via

$$p_0(|\psi_a\rangle|\psi_b\rangle, O) = \text{Tr}[\rho^{\text{fin}} \cdot (|0\rangle\langle 0| \otimes I_{2N})] = \begin{cases} \frac{1}{2}, & \text{if } a \neq b, \\ \frac{1}{2} + \frac{1}{2} \text{Tr}[|\psi_a\rangle\langle\psi_a| O], & \text{if } a = b, \end{cases}$$

where the derangement operator  $D_2$  filters the asymmetric components of  $\rho^{\otimes 2}$  to include only permutation-symmetric parts such as  $|\psi_a\rangle|\psi_a\rangle$ . Then we can arrive at

$$\begin{aligned} 2p_0(\rho, O) - 1 &= (1 - \epsilon)^2 (1 + \langle \psi | O | \psi \rangle) + 2\epsilon(1 - \epsilon) \sum_k + \epsilon^2 \sum_{k,k'} \lambda_k \lambda_{k'} + \epsilon^2 \sum_k \langle \psi_k | O | \psi_k \rangle - 1 \\ &= (1 - \epsilon)^2 - 1 + \text{Tr}[\rho^2 O] + 2 \sum_k \lambda_k \epsilon (1 - \epsilon) + \epsilon^2 \sum_{k,k'} \lambda_k \lambda_{k'} \\ &= \text{Tr}[\rho^2 O]. \end{aligned} \quad (\text{S5})$$

## NOISY VIRTUAL DISTILLATION UNDER PAULI GATE NOISE

In the maintext, we consider the stochastic Pauli gate noise  $\mathcal{E}_m^P(\rho) = (1 - p_m)\rho + p_m \sum_{s=1}^{4^m - 1} \delta_s^m P_s^m \rho P_s^m$ , where  $p_m \geq 0$  is the Pauli error rate and the coefficients  $\{\delta_s^m\}_s$  of the  $m$ -qubit Pauli error terms  $\{P_s^m\}_s$  satisfies  $\delta_s^m \geq 0, \sum_s \delta_s^m = 1$ .

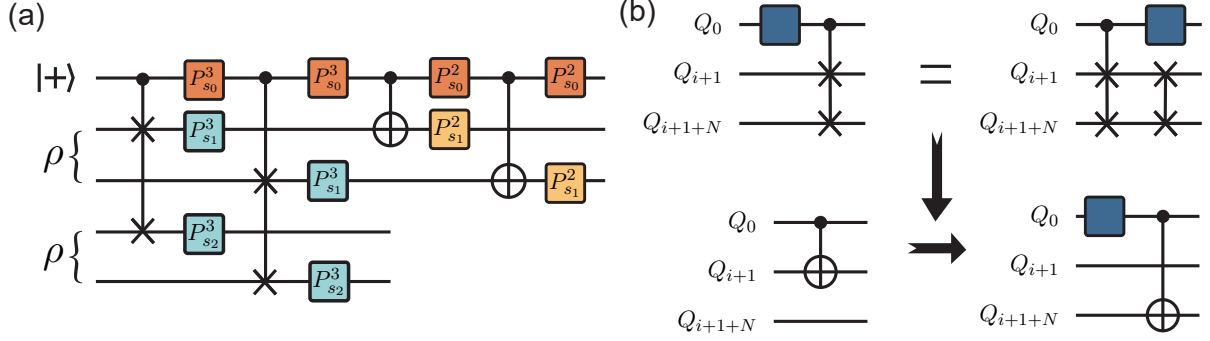


FIG. S1: (a) The 2-qubit and 3-qubit Pauli gate noise in the second-order VD circuit. (b) The effect of the  $\sigma_x$  or  $\sigma_y$  Pauli error (blue square) acting on the controlled qubit  $Q_0$  of the CSWAP gate where we denote the  $j$ -th qubit of the VD circuit as  $Q_j$ . As  $(\sigma_x(\sigma_y) \otimes I \otimes I) \cdot \text{CSWAP} = \text{CSWAP} \cdot (\sigma_x(\sigma_y) \otimes \text{SWAP})$  which introduces a SWAP gate in the qubit  $Q_{i+1}$  and  $Q_{i+1+N}$ , it leads to the transformation of controlled Pauli gate  $\text{CO}_{i+1}$  to  $\text{CO}_{i+1+N}$ .

We denote the  $m$ -qubit ( $m=2,3$ ) Pauli error term as  $P_s^m = \sum_{j=0}^{m-1} P_{s_j}^m$  where  $P_{s_j}^m$  is from the single-qubit Pauli group  $\{I, \sigma_x, \sigma_y, \sigma_z\}^{\otimes m}$ . We now will provide the details of the noisy virtual distillation (VD) under Pauli gate noise in the VD circuit in this section.

We assume local Pauli gate noise, meaning that the gate noise only affects the qubits on which the multi-qubit gate applies. Hence only 3-qubit and 2-qubit Pauli gate noise act on CSWAP gate and controlled Pauli gate, respectively. We define the noisy CSWAP gate  $\widetilde{\text{CSWAP}}_{i,t}$  and controlled Pauli gate  $\widetilde{\text{CO}}_{i_j}$  as

$$\widetilde{\text{CSWAP}}_{i,t} = \mathcal{E}_3^P \cdot \text{CSWAP}_{i,t}, \quad \widetilde{\text{CO}}_{i_j} = \mathcal{E}_2^P \cdot \text{CO}_{i_j}, \quad (\text{S6})$$

as illustrated in the Fig. S1(a). As we solely measure the ancilla qubit  $Q_0$ , it is essential to consider how the Pauli gate noise in the VD circuit affects the measurement outcomes of  $Q_0$ .

*The noise in the CSWAP gate chain*— As the  $N$  CSWAP gates in the VD circuit only share their controlled qubit  $Q_0$ , only the first qubit of the Pauli error term  $P_{s_0}^3$  can influence its following CSWAP gates. Then we can investigate the impact of Pauli terms in the form of  $P_{s_0}^3 \otimes I \otimes I$  before the CSWAP gate,

$$\text{CSWAP} \cdot (P_{s_0}^3 \otimes I \otimes I) = \begin{cases} (P_{s_0}^3 \otimes I \otimes I) \cdot \text{CSWAP}, & \text{if } P_{s_0}^3 = \sigma_z, I \\ (P_{s_0}^3 \otimes \text{SWAP}) \cdot \text{CSWAP}, & \text{if } P_{s_0}^3 = \sigma_x, \sigma_y, \end{cases}$$

which means that the  $\sigma_x$  or  $\sigma_y$  Pauli error occurring on the ancilla qubit  $Q_0$  can generate a undesired SWAP gate on the data qubits for each CSWAP gate behind it. Due to the light-cone principle, not all erroneous SWAP gates will affect the measurement outcome. When the SWAP gate acting on  $(i+1, i+1+N)$  meets  $i \in \mathcal{I}_k$ , it will lead to the transformation of the corresponding controlled Pauli gate from  $\text{CO}_{i+1}$  to  $\text{CO}_{i+1+N}$ , as demonstrated in Fig. S1(b). This can further result in a portion of single-qubit Pauli terms of  $O$ , which originally act only on the register corresponding to the first copy of  $\rho$ , also affecting the second register. We define  $O = O_1 + O_2$  and  $i = 1, 2$  refers to the index of the register which the operator  $O_i$  acts on. Then the final density matrix turns to

$$\tilde{\rho}^{\text{fin}} = \frac{1}{2} (|+\rangle|\psi_a\rangle|\psi_b\rangle\langle +| \langle \psi_a| \langle \psi_b| + |-\rangle O_1 |\psi_b\rangle O_2 |\psi_a\rangle \langle -| \langle \psi_b| O_1 \langle \psi_a| O_2 + |+\rangle|\psi_a\rangle|\psi_b\rangle \langle -| \langle \psi_b| O_1 \langle \psi_a| O_2 + |-\rangle O_1 |\psi_b\rangle O_2 |\psi_a\rangle \langle +| \langle \psi_a| \langle \psi_b|), \quad (\text{S7})$$

and the noisy probability  $\tilde{p}_0(|\psi_a\rangle|\psi_a\rangle, O)$  becomes

$$\tilde{p}_0(|\psi_a\rangle|\psi_b\rangle, O) = \text{Tr}[\tilde{\rho}^{\text{fin}} \cdot (|0\rangle\langle 0| \otimes I_{2N})] = \begin{cases} \frac{1}{2}, & \text{if } a \neq b, \\ \frac{1}{2} + \frac{1}{2} \text{Tr}[|\psi_a\rangle\langle \psi_a| O_1] \cdot \text{Tr}[|\psi_a\rangle\langle \psi_a| O_2], & \text{if } a = b. \end{cases}$$

Hence, the noisy estimation of  $\text{Tr}[\rho^2 O]$  contaminated by the undesired SWAP gate caused by the  $\sigma_x$  or  $\sigma_y$  Pauli error



on the ancilla is

$$\begin{aligned}
2\tilde{p}_0(\rho, O) - 1 &= (1 - \epsilon)^2(1 + \text{Tr}[\psi\rangle\langle\psi|O_1] \cdot \text{Tr}[\psi\rangle\langle\psi|O_2]) + 2\epsilon(1 - \epsilon) \sum_k \lambda_k + \\
&\quad \epsilon^2 \sum_{k,k'} \lambda_k \lambda_{k'} + \epsilon^2 \sum_k \lambda_k \text{Tr}[\psi_k\rangle\langle\psi_k|O_1] \cdot \text{Tr}[\psi_k\rangle\langle\psi_k|O_2] - 1 \\
&= (1 - \epsilon)^2 \text{Tr}[\psi\rangle\langle\psi|O_1] \cdot \text{Tr}[\psi\rangle\langle\psi|O_2] + \epsilon^2 \sum_k \lambda_k \text{Tr}[\psi_k\rangle\langle\psi_k|O_1] \cdot \text{Tr}[\psi_k\rangle\langle\psi_k|O_2].
\end{aligned} \tag{S8}$$

*The noise in the controlled Pauli gate chain*— We then turn our attention to the pauli gate noise in the controlled Pauli gates, along with the residual Pauli noise in the CSWAP gate chain which commutes with the CSWAP gate chain. As the controlled Pauli gate chain is Clifford which conserve the Pauli group, we can serve these Pauli errors as a  $(2N + 1)$ -qubit stochastic Pauli noise channel which acts after the final density matrix  $\rho^{\text{fin}}$ . We consider the effect of the single-qubit Pauli error term  $P_{s_0}$ , it gives

$$\tilde{p}_0(|\psi_a\rangle|\psi_b\rangle, O) = \begin{cases} \frac{1}{2}, & \text{if } a \neq b, \text{ or } a = b \text{ and } P_{s_0} = \sigma_y, \\ \frac{1}{2} + \frac{1}{2}\text{Tr}[|\psi_a\rangle\langle\psi_a|O], & \text{if } a = b \text{ and } P_{s_0} = I, \sigma_x, \\ \frac{1}{2} + \frac{1}{2}\text{Tr}[|\psi_a\rangle\langle\psi_a|O], & \text{if } a = b \text{ and } P_{s_0} = \sigma_z, \end{cases}$$

and then the noisy estimation is

$$2\tilde{p}_0(\rho, O) - 1 = \begin{cases} \text{Tr}[\rho^2 O], & \text{if } P_{s_0} = I, \sigma_x, \\ 0, & \text{if } P_{s_0} = \sigma_y, \\ -\text{Tr}[\rho^2 O], & \text{if } P_{s_0} = \sigma_z. \end{cases} \equiv a \text{Tr}[\rho^2 O],$$

where the parameter  $a$  is  $\rho$ -independent and only determined by the structure of the VD circuit and the noise level of the Pauli gate noise in the VD circuit.

*The outcome of noisy virtual distillation*— From above discussions, it can be inferred that the undesired SWAP errors due to the  $\sigma_x, \sigma_y$  errors on the ancilla qubit  $Q_0$  can lead to a partial shift of the Pauli observable  $O$  from register 1 to register 2, while the remaining Pauli errors result in multiplying the shifted expectation value by a parameter independent of  $\rho$ . When the erroneously generated SWAP gates separates  $O$  into  $O_1$  and  $O_2$ , which reside in registers 1 and 2 respectively, we can obtain a similar expression for  $\tilde{p}_0(|\psi_a\rangle|\psi_a\rangle, O)$  as

$$\tilde{p}_0(|\psi_a\rangle|\psi_a\rangle, O) = \begin{cases} \frac{1}{2} + \frac{1}{2}\langle\psi_a|O_1|\psi_a\rangle \cdot \langle\psi_a|O_2|\psi_a\rangle, & \text{if } P_{s_0} = I, \sigma_x, \\ \frac{1}{2}, & \text{if } P_{s_0} = \sigma_y, \\ \frac{1}{2} - \frac{1}{2}\langle\psi_a|O_1|\psi_a\rangle \cdot \langle\psi_a|O_2|\psi_a\rangle, & \text{if } P_{s_0} = \sigma_z, \end{cases}$$

However, the  $\sigma_x$  and  $\sigma_y$  errors on the ancilla qubit  $Q_0$  also cancel each other out, making it difficult to infer the number of the unwanted SWAPs generated based on the occurrences of  $\sigma_x, \sigma_y$  errors. Therefore, we combine similar terms of expectation values resulting from different Pauli error terms based on the number of unwanted SWAPs in the VD circuit. Then the outcome obtained from the noisy VD circuit can be represented as a function that

$$2\tilde{p}_0(\rho, O) - 1 = \sum_{j=0}^{\lceil \frac{k}{2} \rceil} \sum_{t=0}^{\binom{k}{j}-1} a_{j,t}^k(p_2, p_3, O) A_j(t), \tag{S9}$$

where  $j$  represents the total number of SWAP errors that lead to nontrivial terms of  $O$  being transferred out of register 1, corresponding to  $\binom{k}{j}$  situations. And  $t$  refers to the indices of these situations. It is worth noting that when  $k$  is even and  $j = k/2$ , the number of all the possible combinations of  $O_1$  and  $O_2$  is  $\binom{k}{j}/2$ . We do not make specific mention of this here in order to maintain the uniformity in the expression of  $2\tilde{p}_0(\rho, O) - 1$ .

**CIRCUIT-NOISE-RESILIENT VIRTUAL DISTILLATION UNDER GENERAL MARKOVIAN NOISE MODEL**

**The proof for the full resilience to noise in the VD circuit for the CNR-VD**

In the maintext we have defined the effective noise  $\mathcal{E}^{\text{eff}}$  of the VD circuit, then the noisy probability  $\tilde{p}_0(\rho, O)$  of measuring zero state in the ancilla is

$$\tilde{p}_0(\rho, O) = \text{Tr}[\mathcal{E}^{\text{eff}}\mathcal{U}(|+\rangle\langle+| \otimes \rho^{\otimes n})(|0\rangle\langle 0| \otimes I_{nN})], \quad (\text{S10})$$

here the operator  $\mathcal{U}$  refers to the controlled- $D_n$ , controlled- $O$  and the Hadamard gate  $H$ . We have defined the CNR-VD estimator as

$$\hat{O}_{\text{CNR-VD}}(\rho) = \frac{\hat{O}_{\text{VD}}(\rho)}{\hat{O}_{\text{VD}}(s)}, \quad (\text{S11})$$

when the effective noise  $\mathcal{E}^{\text{eff}}$  satisfies any of these two conditions:

- There exists a set of Kraus operators such that: each Kraus operator  $K_i = K_i^{\text{R}} \otimes K_i^{\text{D}}$  of  $\mathcal{E}^{\text{eff}}$  is separate into subsystems  $\rho^{\text{R}}$  and  $\rho^{\text{D}}$ , along with unitary  $K_i^{\text{R}}$  and  $K_i^{\text{D}}$ .
- $\mathcal{E}^{\text{eff}} = \mathcal{E}^{\text{eff,R}} \otimes \mathcal{E}^{\text{eff,D}}$ , along with the single-qubit unital noise channel  $\mathcal{E}^{\text{eff,R}}$  and the CPTP noise channel  $\mathcal{E}^{\text{eff,D}}$ ,

then the CNR-VD estimator  $\hat{O}_{\text{CNR-VD}}(\rho)$  can reduce the error in the expectation value induced by  $\mathcal{E}^{\text{eff}}$ .

*Proof for Condition 1.*—For simplicity, we take second-order VD and we assume that this two copies of noisy state are the same. Then the tensor product of the state  $\rho^{\otimes 2}$  can be written as a linear combination of four types of pure state terms as shown in Eq. S1:  $|\psi\rangle|\psi\rangle$ ,  $|\psi\rangle|\psi_k\rangle$ ,  $|\psi_k\rangle|\psi\rangle$  and  $|\psi_k\rangle|\psi_{k'}\rangle$ . Then we can decompose the  $\tilde{p}_0(\rho, O)$  in Eq. S10 as  $\tilde{p}_0(\rho, O) = (1 - \epsilon)^2 \tilde{p}_0(|\psi\rangle|\psi\rangle, O) + \epsilon(1 - \epsilon) \sum_k \lambda_k [\tilde{p}_0(|\psi\rangle|\psi_k\rangle, O) + \tilde{p}_0(|\psi_k\rangle|\psi\rangle, O)] + \epsilon^2 \sum_{k,k'} \lambda_k \lambda_{k'} \tilde{p}_0(|\psi_k\rangle|\psi_{k'}\rangle, O)$ . When the effective noise  $\mathcal{E}^{\text{eff}}$  is unital noise channel and each Kraus operator conforms to  $K_i = K_i^{\text{R}} \otimes K_i^{\text{D}}$  along with unitary  $K_i^{\text{R}}$  and  $K_i^{\text{D}}$ , then the expression of  $\tilde{p}_0(|\psi\rangle|\psi\rangle^{\otimes 2}, O)$  in Eq. S21 turns to

$$\begin{aligned} \tilde{p}_0(|\psi\rangle|\psi\rangle, O) &= \frac{1}{2} \text{Tr}[\mathcal{E}^{\text{eff}}(\mathcal{U}(|+\rangle|\psi\rangle|\psi\rangle) \cdot \mathcal{U}(|+\rangle|\psi\rangle|\psi\rangle)^\dagger) \cdot (|0\rangle\langle 0| \otimes I_{2N})] \\ &= \frac{1}{2} \text{Tr}[\mathcal{E}^{\text{eff}}(|+\rangle\langle+| \otimes |\psi\rangle|\psi\rangle\langle\psi|\langle\psi|) \cdot (|0\rangle\langle 0| \otimes I_{2N})] + \frac{1}{2} \text{Tr}[\mathcal{E}^{\text{eff}}(|-\rangle\langle-| \otimes |\psi\rangle O |\psi\rangle\langle\psi| O \langle\psi|) \\ &\quad \cdot (|0\rangle\langle 0| \otimes I_{2N})] + \frac{1}{2} \text{Tr}[\mathcal{E}^{\text{eff}}(|+\rangle\langle-| \otimes |\psi\rangle|\psi\rangle\langle\psi| O \langle\psi|) \cdot (|0\rangle\langle 0| \otimes I_{2N})] \\ &\quad + \frac{1}{2} \text{Tr}[\mathcal{E}^{\text{eff}}(|-\rangle\langle+| \otimes |\psi\rangle O |\psi\rangle\langle\psi| \langle\psi|) \cdot (|0\rangle\langle 0| \otimes I_{2N})] \\ &= \frac{1}{2} \sum_i \text{Tr}[(K_i^{\text{R}}|+\rangle\langle+|K_i^{\text{R}\dagger})|0\rangle\langle 0|] \cdot \text{Tr}[K_i^{\text{D}}|\psi\rangle\langle\psi|^{\otimes 2}K_i^{\text{D}\dagger}] \\ &\quad + \frac{1}{2} \sum_i \text{Tr}[(K_i^{\text{R}}|-\rangle\langle-|K_i^{\text{R}\dagger})|0\rangle\langle 0|] \cdot \text{Tr}[K_i^{\text{D}}(O|\psi\rangle\langle\psi|O)^{\otimes 2}K_i^{\text{D}\dagger}] \\ &\quad + \frac{1}{2} \sum_i \text{Tr}[(K_i^{\text{R}}|+\rangle\langle-|K_i^{\text{R}\dagger})|0\rangle\langle 0|] \cdot \text{Tr}[K_i^{\text{D}}(|\psi\rangle\langle\psi|O \otimes |\psi\rangle\langle\psi|)K_i^{\text{D}\dagger}] \\ &\quad + \frac{1}{2} \sum_i \text{Tr}[(K_i^{\text{R}}|-\rangle\langle+|K_i^{\text{R}\dagger})|0\rangle\langle 0|] \cdot \text{Tr}[K_i^{\text{D}}(|\psi\rangle\langle\psi| \otimes (|\psi\rangle\langle\psi|O))K_i^{\text{D}\dagger}] \\ &= \frac{1}{2} \sum_i \text{Tr}[(K_i^{\text{R}}IK_i^{\text{R}\dagger})|0\rangle\langle 0|] + \frac{1}{2} \text{Tr}[|\psi\rangle\langle\psi|O] \sum_i \text{Tr}[(K_i^{\text{R}}ZK_i^{\text{R}\dagger})|0\rangle\langle 0|] \\ &:= \frac{1}{2} + b \text{Tr}[|\psi\rangle\langle\psi|O], \end{aligned} \quad (\text{S12})$$

where we use the fact that the unitary Kraus operator meeting  $K_i^{\text{R}}K_i^{\text{R}\dagger} = I$ . And for other three pure state terms, the same approach can be employed for computation, yielding the following result:

$$\begin{aligned} \tilde{p}_0(|\psi\rangle|\psi_k\rangle, O) &= a, \\ \tilde{p}_0(|\psi_k\rangle|\psi\rangle, O) &= a, \end{aligned} \quad (\text{S13})$$

$$\tilde{p}_0(|\psi_k\rangle|\psi_{k'}\rangle, O) = \begin{cases} a, & \text{if } k \neq k' \\ a + b\text{Tr}[|\psi_k\rangle\langle\psi_k|O], & \text{else.} \end{cases}$$

Thus we can obtain the expression of  $\tilde{p}_0(\rho, O)$  as

$$\begin{aligned} \tilde{p}_0(\rho, O) &= (1 - \epsilon)^2 \left( \frac{1}{2} + b\text{Tr}[|\psi\rangle\langle\psi|O] \right) + \epsilon(1 - \epsilon) + \epsilon^2 \left( \frac{1}{2} + b \sum_k \lambda_k^2 \text{Tr}[|\psi_k\rangle\langle\psi_k|O] \right) \\ &= \frac{1}{2} + b \left( (1 - \epsilon)^2 \text{Tr}[|\psi\rangle\langle\psi|O] + \epsilon^2 \sum_k \lambda_k^2 \text{Tr}[|\psi_k\rangle\langle\psi_k|O] \right) \\ &= \frac{1}{2} + b\text{Tr}[\rho^2 O]. \end{aligned} \quad (\text{S14})$$

Then we can deduce that

$$\frac{2\tilde{p}_0(\rho, O) - 1}{2\tilde{p}_0(s, O) - 1} = \text{Tr}[\rho^2 O]. \quad (\text{S15})$$

Similarly, it can be obtained that

$$\frac{2\tilde{p}_0(\rho, I) - 1}{2\tilde{p}_0(s, I) - 1} = \text{Tr}[\rho^2]. \quad (\text{S16})$$

Then in this situation, the simplified CNR-VD estimator comply with

$$\hat{O}_{\text{CNR-VD}} = \frac{2\tilde{p}_0(\rho, O) - 1}{2\tilde{p}_0(\rho, I) - 1} \cdot \frac{2\tilde{p}_0(s, O) - 1}{2\tilde{p}_0(s, I) - 1} = \frac{\hat{O}_{\text{VD}}(s)}{\hat{O}_{\text{VD}}(\rho)} = \frac{\text{Tr}[\rho^2 O]}{\text{Tr}[\rho^2]}, \quad (\text{S17})$$

which can also be easily extended to  $n > 2$ .

*Proof for Condition 2.*—When the effective noise  $\mathcal{E}^{\text{eff}}$  is separate on two subsystems R and D that  $\mathcal{E}^{\text{eff}} = \mathcal{E}^{\text{eff,R}} \otimes \mathcal{E}^{\text{eff,D}}$  along with the single-qubit unital noise channel  $\mathcal{E}^{\text{eff,R}}$  and CPTP noise channel  $\mathcal{E}^{\text{eff,D}}$ , then this yields

$$\begin{aligned} \tilde{p}_0(|\psi\rangle|\psi\rangle, O) &= \frac{1}{2} \text{Tr}[\mathcal{E}^{\text{eff,R}}(|+\rangle\langle+|)|0\rangle\langle 0|] \cdot \text{Tr}[\mathcal{E}^{\text{eff,D}}(|\psi\rangle\langle\psi|^{\otimes 2})] \\ &\quad + \frac{1}{2} \text{Tr}[\mathcal{E}^{\text{eff,R}}(|-\rangle\langle-|)|0\rangle\langle 0|] \cdot \text{Tr}[\mathcal{E}^{\text{eff,D}}((O|\psi\rangle\langle\psi|O)^{\otimes 2})] \\ &\quad + \frac{1}{2} \text{Tr}[\mathcal{E}^{\text{eff,R}}(|+\rangle\langle-|)|0\rangle\langle 0|] \cdot \text{Tr}[\mathcal{E}^{\text{eff,D}}((|\psi\rangle\langle\psi|O) \otimes |\psi\rangle\langle\psi|)] \\ &\quad + \frac{1}{2} \text{Tr}[\mathcal{E}^{\text{eff,R}}(|-\rangle\langle+|)|0\rangle\langle 0|] \cdot \text{Tr}[\mathcal{E}^{\text{eff,D}}(|\psi\rangle\langle\psi| \otimes (|\psi\rangle\langle\psi|O))] \\ &= \frac{1}{2} \text{Tr}[\mathcal{E}^{\text{eff,R}}(I)|0\rangle\langle 0|] + \frac{1}{2} \text{Tr}[\mathcal{E}^{\text{eff,D}}(Z)|0\rangle\langle 0|] \cdot \text{Tr}[|\psi\rangle\langle\psi|O] \\ &= \frac{1}{2} + b\text{Tr}[|\psi\rangle\langle\psi|O], \end{aligned} \quad (\text{S18})$$

where we use the fact  $\text{Tr}[\mathcal{E}^{\text{eff,D}}(\sigma)] = \text{Tr}[\sigma]$  for the CPTP noise channel  $\mathcal{E}^{\text{eff,D}}$  and any operator  $\sigma$ , and  $\mathcal{E}^{\text{eff,R}}(I) = I$  for the unital noise channel  $\mathcal{E}^{\text{eff,R}}$ . Therefore, through a similar deduction process as condition 1, we can conclude that the Eq. S17 also holds under condition 2.

### CNR-VD estimator with loosen requirement of the effective noise

We also establish other form of the CNR-VD estimator with relaxed requirement. For differentiation, we denote the  $s^+$  and  $s^-$  as the eigenstate of Pauli  $O$  with eigenvalue  $+1$  and  $-1$ , respectively. As for  $O = I$  where only eigenvalue  $+1$  exists, we replace the first copy of  $s^+$  with  $g^0$  ( $g^{\frac{1}{2}}$ ) which satisfies  $|\langle s^+ | g^0 \rangle|^2 = 0$  (and  $|\langle s^+ | g^{\frac{1}{2}} \rangle|^2 = 1/2$ ), and the noisy probability is referred to  $\tilde{p}_0(g^0, I)$  ( $\tilde{p}_0(g^{\frac{1}{2}}, I)$ ). We will utilize these noisy probabilities obtained from both noisy VD and the calibration stage to establish the CNR-VD estimator in the form of

$$\hat{O}_{\text{CNR-VD}}(\rho) = \left( \frac{2\tilde{p}_0(\rho, O) - \tilde{p}_0(s^+, O) - \tilde{p}_0(s^-, O)}{\tilde{p}_0(\rho, I) - \tilde{p}_0(g^0, I)} \right) \times \left( \frac{2(\tilde{p}_0(g^{\frac{1}{2}}, I) - \tilde{p}_0(g^0, I))}{\tilde{p}_0(s^+, O) - \tilde{p}_0(s^-, O)} \right). \quad (\text{S19})$$

We now turn our attention to the precise condition when  $\hat{O}_{\text{CNR-VD}}(\rho)$  exhibits full resilience to the effective noise. We can get the following condition.

**Theorem S1.** *If the effective noise  $\mathcal{E}^{\text{eff}}$  satisfies*

$$\text{Tr}_{1:nN}[\mathcal{E}^{\text{eff}}(\rho^{\text{RD}})] = \sum_i c_i \text{Tr}[\rho^{\text{D}}] \rho_i^{\text{R}}, \quad \text{with } \rho_i^{\text{R}} = \text{Tr}_{1:nN}[K_i(\rho^{\text{R}} \otimes I_{nN})K_i^\dagger], \quad (\text{S20})$$

where  $\text{Tr}_{1:nN}$  denotes the partial trace over qubits from index 1 to  $nN$  and  $c_i$  is some constant which is exclusively associated with  $\mathcal{E}^{\text{eff}}$ , then the CNR-VD estimator  $\hat{O}_{\text{CNR-VD}}(\rho)$  given in Eq. S19 can eliminate the undesired bias in the expectation value caused by  $\mathcal{E}^{\text{eff}}$ .

The criteria of  $\mathcal{E}^{\text{eff}}$  set out in Eq. S20 means that the effective noise does not introduce entanglement between  $\rho^{\text{R}}$  and  $\rho^{\text{D}}$ .

*Proof.*— For the effective noise  $\mathcal{E}^{\text{eff}}$  satisfying the conditions described in theorem 1,  $\tilde{p}_0(|\psi\rangle|\psi\rangle, O)$  equals

$$\begin{aligned} \tilde{p}_0(|\psi\rangle|\psi\rangle, O) &= \frac{1}{2} \text{Tr}[\mathcal{E}^{\text{eff}}(\mathcal{U}(|+\rangle|\psi\rangle|\psi\rangle) \cdot \mathcal{U}(|+\rangle|\psi\rangle|\psi\rangle)^\dagger) \cdot (|0\rangle\langle 0| \otimes I_{2N})] \\ &= \frac{1}{2} \text{Tr}[\mathcal{E}^{\text{eff}}(|+\rangle\langle +| \otimes |\psi\rangle\langle \psi|) \cdot (|0\rangle\langle 0| \otimes I_{2N})] + \frac{1}{2} \text{Tr}[\mathcal{E}^{\text{eff}}(|-\rangle\langle -| \otimes |\psi\rangle\langle \psi|) \cdot (|0\rangle\langle 0| \otimes I_{2N})] \\ &\quad \cdot (|0\rangle\langle 0| \otimes I_{2N}) + \frac{1}{2} \text{Tr}[\mathcal{E}^{\text{eff}}(|+\rangle\langle -| \otimes |\psi\rangle\langle \psi|) \cdot (|0\rangle\langle 0| \otimes I_{2N})] \\ &\quad + \frac{1}{2} \text{Tr}[\mathcal{E}^{\text{eff}}(|-\rangle\langle +| \otimes |\psi\rangle\langle \psi|) \cdot (|0\rangle\langle 0| \otimes I_{2N})] \\ &= \frac{1}{2} \sum_i c_i \text{Tr}[K_i((|+\rangle\langle +| + |-\rangle\langle -|) \otimes I_{2N})K_i^\dagger \cdot (|0\rangle\langle 0| \otimes I_{2N})] \\ &\quad + \frac{1}{2} \text{Tr}[|\psi\rangle\langle \psi|O] \cdot \sum_i c_i \text{Tr}[K_i((|+\rangle\langle -| + |-\rangle\langle +|) \otimes I_{2N})K_i^\dagger \cdot (|0\rangle\langle 0| \otimes I_{2N})] \\ &= \frac{1}{2} \sum_i c_i \text{Tr}[K_i K_i^\dagger \cdot (|0\rangle\langle 0| \otimes I_{2N})] + \frac{1}{2} \text{Tr}[|\psi\rangle\langle \psi|O] \cdot \sum_i c_i \text{Tr}[K_i((Z \otimes I_{2N})K_i^\dagger \cdot (|0\rangle\langle 0| \otimes I_{2N}))] \\ &:= a + b \text{Tr}[|\psi\rangle\langle \psi|O], \end{aligned} \quad (\text{S21})$$

where the noise parameters  $a$  and  $b$  are unrelated to the input state  $|\psi\rangle\langle \psi|^{\otimes 2}$  since  $c_i$  is only exclusively relative with  $\mathcal{E}^{\text{eff}}$ . Thus we can obtain the expression of  $\tilde{p}_0(\rho, O)$  in the similar way as in Eq. S14

$$\begin{aligned} \tilde{p}_0(\rho, O) &= (1 - \epsilon)^2(a + b \text{Tr}[|\psi\rangle\langle \psi|O]) + 2a\epsilon(1 - \epsilon) + \epsilon^2(a + b \sum_k \lambda_k^2 \text{Tr}[|\psi\rangle\langle \psi_k|O]) \\ &= a + b \left( (1 - \epsilon)^2 \text{Tr}[|\psi\rangle\langle \psi|O] + \epsilon^2 \sum_k \lambda_k^2 \text{Tr}[|\psi\rangle\langle \psi_k|O] \right) \\ &= a + b \text{Tr}[\rho^2 O]. \end{aligned} \quad (\text{S22})$$

When we input the eigenstate  $s^+$  ( $s^-$ ) of the Pauli observable  $O$  with eigenvalue 1 (-1), we can obtain  $\tilde{p}_0(s^+, O) = a + b$  ( $\tilde{p}_0(s^-, O) = a - b$ ). As a result, it follows that

$$\frac{2\tilde{p}_0(\rho, O) - \tilde{p}_0(s^+, O) - \tilde{p}_0(s^-, O)}{\tilde{p}_0(s^+, O) - \tilde{p}_0(s^-, O)} = \text{Tr}[\rho^2 O]. \quad (\text{S23})$$

For  $O = I$ , the  $\tilde{p}_0(\rho, I) = a' + b' \text{Tr}[\rho^2]$  and  $\tilde{p}_0(s^+, I) = a' + b'$ . When we replace the first copy of  $s^+$  with  $g^0$ , since  $s^+$  and  $g^0$  are both pure states we can get

$$\tilde{p}_0(g^0, I) = a' + b' |\langle s^+ | g^0 \rangle|^2 = a', \quad (\text{S24})$$

following Eq. S21. And the same way can be used to obtain  $\tilde{p}_0(g^{\frac{1}{2}}, I) = a' + b'/2$ . Then we get

$$\frac{\tilde{p}_0(\rho, I) - \tilde{p}_0(g^0, I)}{2(\tilde{p}_0(g^{\frac{1}{2}}, I) - \tilde{p}_0(g^0, I))} = \text{Tr}[\rho^2], \quad (\text{S25})$$

which means the CNR-VD estimator defined in Theorem 1 satisfies

$$\begin{aligned}\hat{O}_{\text{CNR-VD}}(\rho) &= \frac{2\tilde{p}_0(\rho, O) - \tilde{p}_0(s^+, O) - \tilde{p}_0(s^-, O)}{\tilde{p}_0(\rho, I) - \tilde{p}_0(g^0, I)} \\ &= \frac{2(\tilde{p}_0(g^{\frac{1}{2}}, I) - \tilde{p}_0(g^0, I))}{\tilde{p}_0(s^+, O) - \tilde{p}_0(s^-, O)} = \frac{\text{Tr}[\rho^2 O]}{\text{Tr}[\rho^2]}.\end{aligned}\quad (\text{S26})$$

And this can be easily extended to  $n > 2$  by expanding  $\rho^n$  in terms of the binomial series.

### The variance of the CNR-VD estimator

Since the CNR-VD estimator is in a form of quotient, we can employ the error propagation formula to calculate the variance of the CNR-VD estimator, incorporating the first-order Taylor expansion into the calculation. Consider a function  $Y = A/B$ , where  $A$  and  $B$  are random variables. When  $A$  and  $B$  are mutual independent, we can compute the variance of  $Y$  denoted as  $\text{Var}[Y]$  by

$$\text{Var}[Y] \approx \left(\frac{\mathbb{E}[A]}{\mathbb{E}[B]}\right)^2 \cdot \left(\frac{\text{Var}[A]}{(\mathbb{E}[A])^2} + \frac{\text{Var}[B]}{(\mathbb{E}[B])^2}\right). \quad (\text{S27})$$

Here we only calculate the variance of the CNR-VD estimator in Eq. S11 and we can compute the variance of other version of CNR-VD estimator in the similar way. The variance of the simplified  $\hat{O}_{\text{CNR-VD}}(\rho)$  is

$$\begin{aligned}\text{Var}[\hat{O}_{\text{CNR-VD}}(\rho)] &= \text{Var}\left[\frac{\hat{O}_{\text{VD}}(\rho)}{\hat{O}_{\text{VD}}(s)}\right] \\ &= \left(\frac{\mathbb{E}[\hat{O}_{\text{VD}}(\rho)]}{\mathbb{E}[\hat{O}_{\text{VD}}(s)]}\right)^2 \left(\frac{\text{Var}[\hat{O}_{\text{VD}}(\rho)]}{(\mathbb{E}[\hat{O}_{\text{VD}}(\rho)])^2} + \frac{\text{Var}[\hat{O}_{\text{VD}}(s)]}{(\mathbb{E}[\hat{O}_{\text{VD}}(s)])^2}\right).\end{aligned}\quad (\text{S28})$$

If we assume  $\hat{O}_{\text{VD}}(\rho)$  has the same variance for any input state under the same measurement shots number  $M$ , we can infer that the variance of  $\hat{O}_{\text{CNR-VD}}(\rho)$  scales proportionally to that of  $\hat{O}_{\text{VD}}(\rho)$  by

$$\begin{aligned}\text{Var}[\hat{O}_{\text{CNR-VD}}(\rho)] &= \\ &= \left(\frac{1}{(\mathbb{E}[\hat{O}_{\text{VD}}(s)])^2} + \frac{(\mathbb{E}[\hat{O}_{\text{VD}}(\rho)])^2}{(\mathbb{E}[\hat{O}_{\text{VD}}(s)])^4}\right) \text{Var}[\hat{O}_{\text{VD}}(\rho)] \\ &\leq \left(\frac{(\mathbb{E}[\hat{O}_{\text{VD}}(s)])^2 + 1}{(\mathbb{E}[\hat{O}_{\text{VD}}(s)])^4}\right) \text{Var}[\hat{O}_{\text{VD}}(\rho)],\end{aligned}\quad (\text{S29})$$

where the factor is totally determined by  $\mathbb{E}[\hat{O}_{\text{VD}}(s)]$  which indicates the noise level in the VD circuit.

To investigate the relationship among  $\mathbb{E}[\hat{O}_{\text{VD}}(s)]$ , the qubit number  $N$ , and the order  $n$  more intuitively, we consider the simplest scenario where only local depolarizing gate noise with error rate  $\gamma$  occurs in the circuit. Since the depolarizing noise meets  $\mathcal{E}_\gamma^{\text{dep}}(P) = (1 - \frac{4}{3}\gamma)P$  for non-trivial Pauli terms  $X$ ,  $Y$  and  $Z$ , we can get  $\mathcal{E}[\hat{O}_{\text{VD}}(s)] = \frac{(1 - \frac{4}{3}\gamma)^{(n-1)N+k}}{(1 - \frac{4}{3}\gamma)^{(n-1)N}} = (1 - \frac{4}{3}\gamma)^k$  and  $k$  is weight of observable  $O$  which is the count of non-trivial Pauli terms in  $O$ . Consequently, we deduce

$$\frac{(\mathbb{E}[\hat{O}_{\text{VD}}(s)])^2 + 1}{(\mathbb{E}[\hat{O}_{\text{VD}}(s)])^4} = \frac{(1 - \frac{4}{3}\gamma)^{2k} + 1}{(1 - \frac{4}{3}\gamma)^{4k}} = \frac{1}{(1 - \frac{4}{3}\gamma)^{2k}} + \frac{1}{(1 - \frac{4}{3}\gamma)^{4k}}. \quad (\text{S30})$$

We perform a Taylor expansion around  $\gamma = 0$ , truncating the series at  $o(\gamma^2)$ ,

$$\left(1 - \frac{4}{3}\gamma\right)^{-k} = 1 + \frac{4}{3}k\gamma + \frac{8k(k+1)}{9}\gamma^2. \quad (\text{S31})$$

Thus, we arrive at

$$\frac{(\mathbb{E}[\hat{O}_{\text{VD}}(s)])^2 + 1}{(\mathbb{E}[\hat{O}_{\text{VD}}(s)])^4} \approx 2 + (8\gamma + \frac{16}{3}\gamma^2)k + \frac{160}{9}\gamma^2 k^2, \quad (\text{S32})$$



$q_0$	$q_1$	$q_2$	$q_0$	$q_1$	$q_2$
$I$	$I$	$I$	$Z$	$I$	$I$
$I$	$X$	$X$	$Z$	$X$	$X$
$I$	$Y$	$Y$	$Z$	$Y$	$Y$
$I$	$Z$	$Z$	$Z$	$Z$	$Z$

FIG. S2: The chosen subset of 3-qubit Pauli operators which are preserved by CSWAP gate under conjugation.

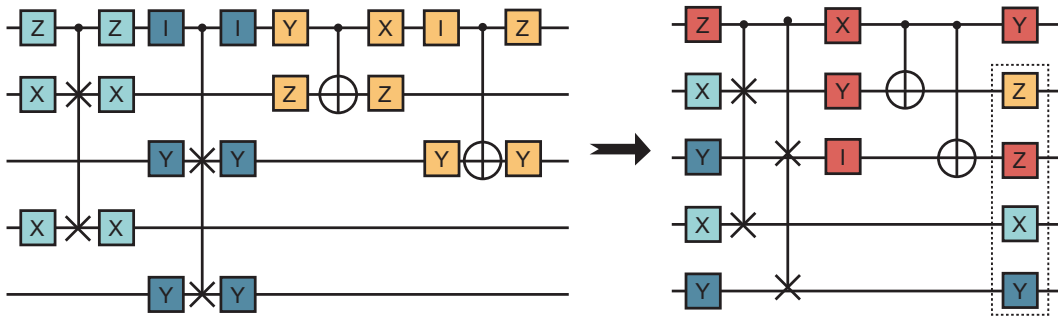


FIG. S3: The compilation of Pauli twirling gates for second-order VD circuit. In the compilation process, the twirling gates for the CSWAP gate are randomly selected from Fig. S2. Due to the property of these chosen Pauli gates that remain unchanged by the CSWAP gate under conjugation, they can be compiled with the Pauli gates before and after the CSWAP chain. Only additional three layers of Pauli gates are needed for RC after the compilation. Furthermore, the first layer of Pauli gates in the right figure can also be compiled together with the single-qubit gates in the state preparation circuit of the input state. And in the third layer of Pauli gates, only the Pauli gate on the first qubit needs to apply since we only perform measurements on the first qubit.

which entails that the scaling factor of variance for the CNR-VD estimator remains uncorrelated with the order of VD, and when the level of gate noise is minimal, the scaling factor exhibits a polynomial growth with the weight  $k$  of the observable.

### THE IMPLEMENTATION OF THE RANDOMIZED COMPILING EMPLOYED IN THE CNR-VD

In the maintext, we employed randomized compilation (RC) technique in computing the CNR-VD estimator to come close to the main assumption of stochastic Pauli gate noise. In this section, we will provide a detailed explanation of the procedure.

Traditional RC is typically performed before and after the noisy multi-qubit gates, and newly generated circuits exhibit logical equivalence with their original counterparts. In practice, it is customary to select a fixed number of circuit with different random twirling instances and perform a certain number of measurements for each circuit, rather than resampling random twirling instance for per measurement shot. We will use second-order VD for all subsequent discussions in this section. We can perform RC on the CSWAP chain and controlled- $O$  chain separately. For the controlled- $O$  chain which is Clifford, we can randomly select a  $2N + 1$ -qubit Pauli operator  $P$  and calculate the corresponding conjugated Pauli gate  $P^{\text{twrl}}$  by

$$P^{\text{twrl}} = CO \cdot P \cdot CO^\dagger, \quad (\text{S33})$$

where  $CO$  represents the controlled- $O$  chain. When it comes to the CSWAP chain, as the CSWAP gate are not Clifford, the Pauli operator conjugated by the CSWAP gate may not still be a Pauli operator. We choose 8 Pauli gates from 3-qubit Pauli group in Fig. S2 which remain unchanged after being conjugated by CSWAP gate. Since the CSWAP gates in the CSWAP chain only share the control qubit, we can readily derive the form of Pauli operators

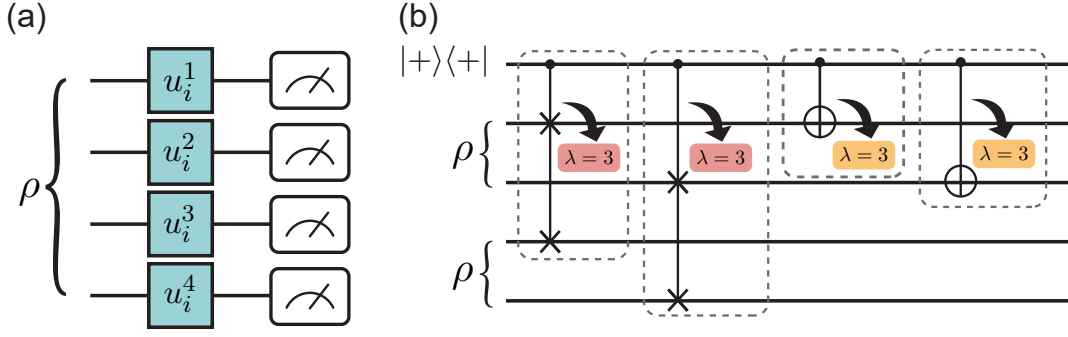


FIG. S4: **The visualization presented depicts the process of 4-qubit shadow distillation (SD) and 2-qubit VD integrated with zero-noise extrapolation (ZNE-VD) for observable  $X^{\otimes 2}$ .** (a) Random single-qubit Clifford gate  $u_i^{(j)}$  ( $j = 1, 2, 3, 4$ ) is applied to each qubit of  $\rho$ , followed by the computation of  $\frac{\text{Tr}[\rho^2 X^{\otimes 2}]}{\text{Tr}[\rho^2]}$  through shadow estimation utilizing the measurement outcomes of a set of random gates  $\{U_i = \prod_{j=1}^4 u_i^{(j)}\}_i$ . (b) The noise level is amplified three times for zero-noise extrapolation, with an amplification error 94%.

preserved by the CSWAP gate under conjugation

$$T = T^{\text{twrl}} = \{I, Z\}^0 \otimes \sum_{j=0}^{N-1} P^{j+1} P^{j+1+N}, \quad (\text{S34})$$

where  $P$  is randomly chosen Pauli operator and the superscript denotes the qubit on which the operator acts. It is possible to compile the Pauli twirling gates chosen for the CSWAP gate with the surrounding Pauli gates, due to the property of remaining unchanged under conjugation with the CSWAP gate. After compilation only three additional layers of Pauli gates are needed for implementing RC in the VD circuit. Additionally, the first layer of Pauli gates in the right figure can be compiled together with the single-qubit gates in the state preparation circuit of the input state. In the third layer of Pauli gates, it is only necessary to apply the Pauli gate on the first qubit, as we are only performing measurements on this qubit.

## DETAILS OF NUMERICAL SIMULATIONS

### The implementation of shadow distillation and VD integrated with zero-noise extrapolation

In the numerical simulations conducted in this maintext, we compare the CNR-VD with two common VD-based methods which are designed against noise in the VD circuit, namely Shadow Distillation and VD integrated with Zero-Noise Extrapolation. In this section, we will provide a comprehensive description of the implementation process for these two methods, and we only use second-order VD in this simulations. The illustration of these two methods are given in Fig. S4

#### Shadow Distillation

Shadow Distillation (SD) is one of the variants of VD which use shadow estimation technique to estimate the unlinear function  $\frac{\text{Tr}[\rho^2 O]}{\text{Tr}[\rho^2]} = \frac{\text{Tr}[D_2(\rho \otimes (\rho O))]}{\text{Tr}[D_2 \rho \otimes \rho]}$  of  $\rho$ . In the SD, we treat the operator  $D_2(I \otimes O)$  ( $D_2$ ) as an observable. By randomly choosing  $N_u$  local Clifford gates  $\{U_i\}_i$ , we obtain the corresponding shadow  $\bar{\rho}_i$  from  $N_s$  measurement outcomes for each  $U_i$ . Then we can use the estimator  $\hat{O}_{\text{SD}}(\rho) = \hat{O}_{\text{SD}}^{\text{num}}(\rho) / \hat{O}_{\text{SD}}^{\text{den}}(\rho)$  to compute the error-mitigated expectation value where

$$\hat{O}_{\text{SD}}^{\text{num}}(\rho) = \frac{1}{N_u(N_u - 1)} \sum_{i \neq i'} \text{Tr}[D_2 \bar{\rho}_i \otimes (\bar{\rho}_{i'} O)], \quad (\text{S35})$$

and we can get  $\hat{O}_{\text{SD}}^{\text{den}}(\rho)$  by replacing  $O$  with  $I$ . In our simulations, we set  $N_s = 10$  if the total measurement shots  $M \leq 10^4$ , otherwise  $N_s = 50$ .

*VD integrated with Zero-Noise Extrapolation*

Typical quantum error mitigation methods such as Zero-Noise Extrapolation (ZNE) can also be employed to minimize the noise in the VD circuit, and we denote this method as ZNE-VD. ZNE employs data gathered across varying error rates to develop a model of expectation values, which can be extrapolated to zero noise limit. We use the two-points exponential extrapolation [S1] to calculate  $\text{Tr}[\rho^2 O]$  by

$$\hat{O}_{\text{ZNE-VD}}^{\text{num}}(\rho) = \left( \frac{\hat{O}_{\text{VD}}^\lambda(\rho, \epsilon)}{\hat{O}_{\text{VD}}(\rho, \lambda\epsilon)} \right)^{\frac{1}{\lambda-1}}, \quad (\text{S36})$$

here we employ the denotation that  $\hat{O}_{\text{VD}}^{\text{num}}(\rho, \lambda\epsilon)$  is the estimation of  $\text{Tr}[\rho^2 O]$  under error rate  $\lambda\epsilon$  where  $\lambda \geq 1$  is the amplified coefficient for the original noise level  $\epsilon$ . Then the error-mitigated expectation value of ZNE-VD is computed via  $\hat{O}_{\text{ZNE-VD}}(\rho) = \hat{O}_{\text{ZNE-VD}}^{\text{num}}(\rho) / \hat{O}_{\text{ZNE-VD}}^{\text{num}}(\rho)$ . The noise level of gate noise is amplified by  $\lambda = 3$  with the amplification error 94% [S2]. In the numerical simulations, we also employ RC technique in the VD circuit to enhance the efficacy of ZNE. The implementation of RC is the same as illustrated in Fig. S3.

**Noise model used in the numerical simulations**

In the maintext, we assume that quantum circuits are mainly affected by the multi-qubit gate noise. And we also assume clean readout in the VD-based circuit since it only requires single-qubit measurement on the ancilla qubit. When we perform shadow distillation (SD) and unmitigated estimation, noisy multi-qubit measurements are still needed. Hence we also employ the multi-qubit readout error model in simulations. Moreover, we also configure the state preparation error for the noisy state applied to the VD circuit. In this section, we will provide details of the gate-noise model, multi-qubit readout error model and state preparation error in the following. All the numerical simulations are performed on Cirq [S3, S4].

*Gate noise model*

We employ two types of gate noise model which are the stochastic Pauli gate noise model and the composite gate noise model consisting of depolarizing, phase damping and amplitude damping.

*The stochastic Pauli gate noise.*—We set  $\epsilon$  to be the noise level which is the average error rate for 2-qubit gates. Then we can calculate the Pauli error rate  $p_2 = (\epsilon/(1 - 1/4)) \cdot (1 - 1/16)$  [S5] with randomly chosen Pauli noise parameters  $\{\delta_s^2\}_s$ . We use the same stochastic Pauli noise within each independent experiment including noisy VD and the calibration stage. Taking into consideration that the experimental implementation of the CSWAP gate typically involves the use of 2-qubit gates for compilation, we have adopted the compilation method outlined in Ref [S2], where a minimum of six 2-qubit gates is required to compile the CSWAP gate. Consequently, according to Ref [S5], the process fidelity of the CSWAP gate is six times greater than that of 2-qubit gates under Pauli error rate  $p_2$ . As a result, we are able to calculate that the fidelity of the CSWAP gate is  $\mathcal{F}(\text{CSWAP}) = (1 - p_2)^6$  and derive the corresponding Pauli error rate  $p_3 = 1 - \mathcal{F}(\text{CSWAP}) = 1 - (1 - p_2)^6$ .

*The composite gate noise.*—Given the noise level  $\epsilon$  and the  $m$ -qubit state  $\rho_m$ , we employ  $m$ -qubit depolarizing gate noise

$$\mathcal{E}_{\text{depo}}^m(\rho_m) = (1 - \epsilon_m)\rho_m + \epsilon_m I_m,$$

for  $m$ -qubit gates and the  $\epsilon_m$  is computed in the similar way as the Pauli gate noise. We also utilize single-qubit phase damping  $\mathcal{E}_{\text{phase}}$  and amplitude damping  $\mathcal{E}_{\text{ampl}}$  with the following definitions

$$\mathcal{E}_{\text{phase}} = E_0 \rho_1 E_0^\dagger + E_1 \rho_1 E_1^\dagger$$

and

$$\mathcal{E}_{\text{ampl}} = E_0 \rho_1 E_0^\dagger + E_2 \rho_1 E_2^\dagger$$

where the Kraus operator  $E_0 = \begin{bmatrix} 1 & 0 \\ 0 & \sqrt{1-\epsilon} \end{bmatrix}$ ,  $E_1 = \begin{bmatrix} 0 & 0 \\ 0 & \sqrt{\epsilon} \end{bmatrix}$  and  $E_2 = \begin{bmatrix} 0 & \sqrt{\epsilon} \\ 0 & 0 \end{bmatrix}$ . And the tensor products of  $\mathcal{E}_{\text{phase}}$  and  $\mathcal{E}_{\text{ampl}}$  are set to construct the composite gate noise along with the  $m$ -qubit depolarizing gate noise.

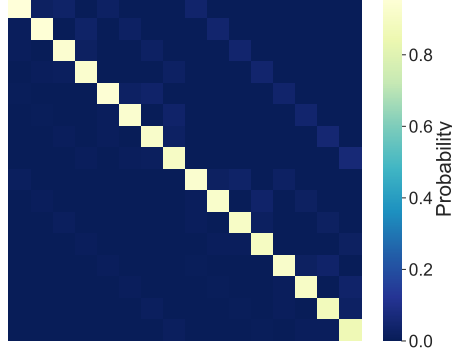


FIG. S5: The 4-qubit transfer matrix obtained from *Zuchongzhi 2.1.*

#### Readout noise model

It is common to assume the classical readout error model where the transfer matrix  $\Lambda$  is employed to describe the transformation between ideal and noisy measurement probability distributions which are denoted as  $\mathbf{p}^{\text{ideal}}$  and  $\mathbf{p}^{\text{noisy}}$

$$\mathbf{p}^{\text{ideal}} = \Lambda^{-1} \mathbf{p}^{\text{noisy}}. \quad (\text{S37})$$

The element  $\Lambda_{\mathbf{x},\mathbf{y}}$  of the response matrix  $\Lambda$  is expressed as

$$\Lambda_{\mathbf{x},\mathbf{y}} = \langle \mathbf{x} | \rho | \mathbf{y} \rangle, \quad \mathbf{x}, \mathbf{y} \in \mathbb{Z}_2^N, \quad (\text{S38})$$

where  $\mathbf{x} \in \mathbb{Z}_2^N$  refers to the measurement outcome. We utilize the Iterative Bayesian Unfolding (IBU) method [S6] to calculate  $\mathbf{p}^{\text{ideal}}$  in order to avoid the direct inversion in Eq. S37, which may produce unphysical probabilities and amplify the statistical uncertainties in  $\Lambda$ . We use 100 IBU iterations and iteration formula for the  $(t+1)$ -th iteration is calculated as follows

$$m_i^{t+1} = \sum_j \frac{\Lambda_{ji} m_i^t}{\sum_k \Lambda_{jk} m_k^t} \times r_j, \quad (\text{S39})$$

where  $m_i$  and  $r_j$  are the  $i$ -th and  $j$ -th terms in the probability estimated by IBU and the  $\mathbf{p}^{\text{noisy}}$ , respectively.

The full transfer matrix  $\Lambda$  we used as readout error is built on the calibration data in *Zuchongzhi 2.1* [S7] as shown in Fig. S5 and the estimated transfer matrix  $\bar{\Lambda}$  for IBU is obtained under the Tensor Product Noise [S8] (TPN) model that  $\bar{\Lambda} = \bar{\Lambda}_1 \otimes \bar{\Lambda}_2 \otimes \dots \otimes \bar{\Lambda}_N$ . The single-qubit transfer matrix  $\bar{\Lambda}_i$  on  $(i-1)$ -th qubit also relies on the calibration data in *Zuchongzhi 2.1*. We use the TPN model because full matrix calibration is exponentially costly. However, this assumption completely ignores the correlated readout error, which leads to additional correlated measurement noise in SD and unmitigated estimation.

#### State preparation noise

In our numerical simulations in the maintext, two types of noisy states are employed. The first is the random state  $\rho_r = (1 - \epsilon)|\psi\rangle\langle\psi| + \epsilon|\psi_e\rangle\langle\psi_e|$  with certain purity  $(1 - \epsilon)^2 + \epsilon^2$ . We set the density matrix  $\rho_r$  as the initial state applied to the VD circuit without specific state preparation circuit. The second is the  $N$ -qubit GHZ state  $|\text{GHZ}\rangle_N = \frac{1}{\sqrt{2}}(|0\rangle^{\otimes N} + |1\rangle^{\otimes N})$ , we use a single-qubit Hadamard gate and  $N - 1$  two-qubit CX gates for state preparation. We add the composite gate noise model to the multi-qubit gates under noise level  $10^{-3}$  in the state preparation circuit, which leads to the state preparation error.

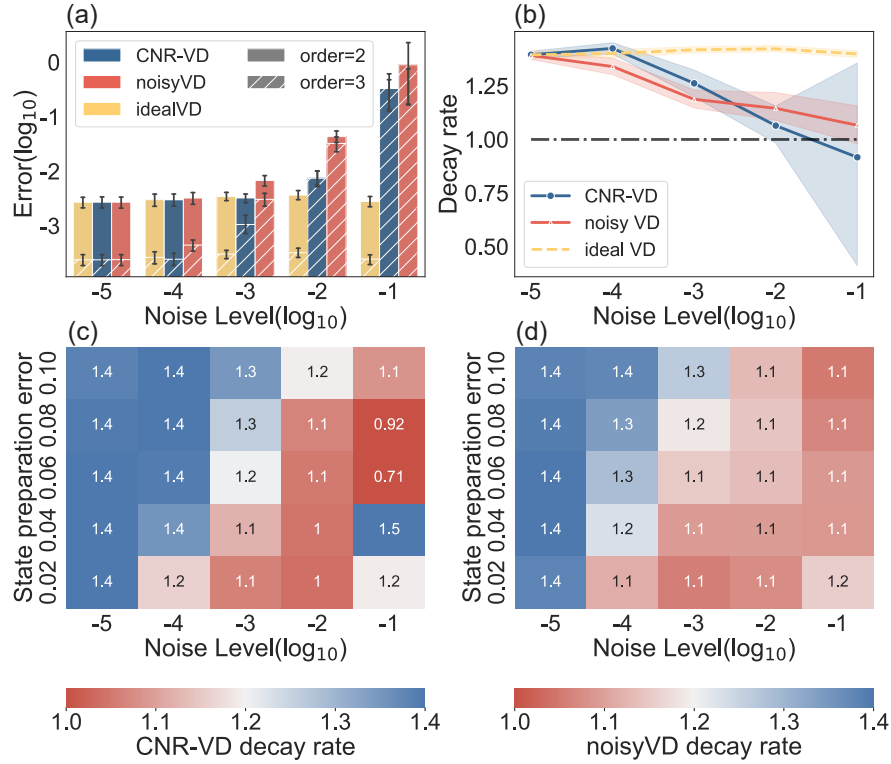


FIG. S6: **Performance on CNR-VD of random noisy states, with different orders of VD.** (a) The complete visualization of the variation in accuracy with order 2,3 and varying noise levels. (b) The decay rate of the expectation value estimation error varying with the noise levels. (c) The heat map of the decay rate for CNR-VD varying with state preparation error rates and noise levels of the VD circuit. (d) The heat map of the decay rate for noisy VD. The displayed data represents the average outcome derived from 50 separate experiments with different random states.

### Relative simulation results

#### *Simulation results for higher order VD*

We focus on the second-order VD in the maintext. Here, we supplement several simulations for random noisy state  $\rho_r$  concerning higher-order VD and explore the relationship between the accuracy of CNR-VD and the increase in the order of VD with order 2 and order 3, noise level in the VD circuit changing from  $10^{-5}$  to  $10^{-1}$  and the state preparation error rate varying from 0.02 to 0.10. Referring to the data illustrated in Fig. S6(a), CNR-VD demonstrates an impressive ability to recover the ideal behavior of VD, with noise level lower than  $10^{-3}$ . However, as the noise level increases, the incremental improvement in accuracy for CNR-VD from increasing the order diminishes gradually, reaching a point at  $10^{-1}$  where the results for order 3 are actually inferior to those for order 2. We can also observe this from Fig. S6(b), where we define the decay rate as the logarithm of the ratio of the accuracy of order 2 to that of order 3. It is obvious that beyond a certain threshold of noise level about  $10^{-2}$ , the cost-effectiveness of increasing the order becomes significantly diminished, to the extent that it may even become lower than that of the noisy VD. We further present a detailed demonstration of the decay rate of CNR-VD and noisy VD as they vary with the changes in noise levels of the VD circuit and state preparation error rates, as shown in Fig. S6(c) and Fig. S6(d).

#### *Detailed simulation results for GHZ state*

In the maintext, we compare the performance on five estimators: CNR-VD, ZNE-VD, SD, noisy VD and unmitigated estimation (Unmit) for  $N$ -qubit GHZ state and Pauli observable  $\sigma_x^{\otimes N}$ , with varying qubit number  $N$  and total shot number  $M$ . The total shot number  $M$  contains all the procedures of the estimators. For instance, CNR-VD takes double circuit instances of noisy VD due to the calibration stage. Moreover, as we employ RC for CNR-VD with 4



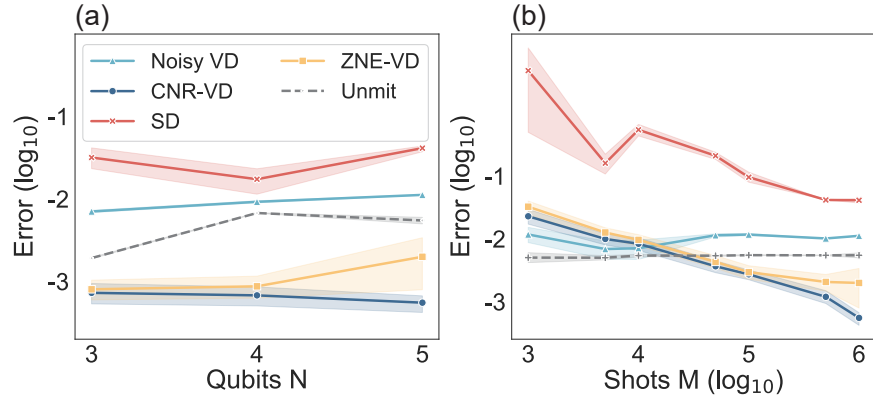


FIG. S7: Accuracy of several VD-based methods for GHZ state, with increasing qubit number  $N$  and shot number  $M$ . The displayed data represents the average outcome derived from 20 separate experiments.

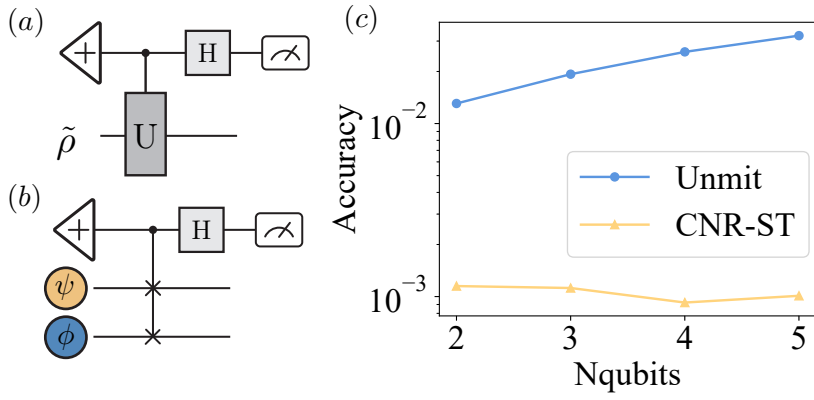


FIG. S8: Coalesced presentation showcasing the circuit of Hadamard-Test and SWAP-Test and the simulation results pertaining to the SWAP-Test. (a) The quantum circuit of Hadamard-Test. (b) The illustration of SWAP-Test to estimate the overlap of two quantum states  $\psi$  and  $\phi$  (c) The simulation results of SWAP-Test with Unmit and CNR-ST. The displayed data represents the average outcome derived from 50 separate experiments, with the error bars indicating the corresponding standard deviation.

random instances, CNR-VD takes 16 circuit instances and the measurement shot number of each circuit instance is  $M/16$ . Here, we illustrate the detailed variation curves of the accuracy of these estimators with respect to  $N$  and  $M$ , as shown in Fig. S7. As discussed in the maintext, the mitigated VD methods including CNR-VD, ZNE-VD and SD introduce additional sampling overhead to mitigate the noise in the VD circuit, leading to poorer results when the total shot number  $M$  is low, to the extent that they are even worse than unmitigated estimation. However, as shown in Fig. S7(b), increasing the total shot number  $M$  can bring sustained benefits to CNR-VD, and when  $M$  exceeds approximately  $5 \times 10^4$ , CNR-VD outperforms unmitigated estimation.

### EXTENSION FOR GENERAL APPLICATIONS

In order to demonstrate the generality of CNR-VD, we perform numerical simulations on a representative application of the Hadamard-Test, namely the SWAP-Test [S9, S10]. SWAP-Test is a fundamental protocol in quantum computing. By swapping the two states via performing CSWAP operators, SWAP-Test enables to estimate the state overlap which provides valuable insights into quantum state comparison and discrimination. We conducted numerical experiments utilizing the SWAP-Test on two randomly generated quantum states  $\psi$  and  $\phi$  as illustrated in Fig. S8(b). We call the SWAP-Test using the CNR estimator as CNR-ST, and the input state  $s$  is  $|0\rangle^{\otimes N}$ . The accuracy are still calculated using the absolute error.

To alleviate the impact of the extreme values of the ideal overlap on the estimation of absolute error, we generated

the pair of random quantum states with a fixed overlap

$$|\psi\rangle = U_R|0\rangle^{\otimes N}, |\phi\rangle = U_R|+\rangle^{\otimes N}, \quad (\text{S40})$$

where the random unitary operator  $U_R$  can maintain the inner product of  $\psi$  and  $\phi$  as  $\langle\psi|\phi\rangle = \langle 0|^{\otimes N} U_R^\dagger U_R |+\rangle^{\otimes N} = \langle 0|^{\otimes N} |+\rangle^{\otimes N} = \frac{1}{2}$ . We conduct simulations on estimating the overlap of random states on qubits with number ranging from 2 to 5 and compare the accuracy between the unmitigated SWAP-Test (Unmit) and CNR-ST. The results are given in Fig. S8(c). This two approaches are implemented with the same number of total measurement shots  $10^6$ . There is clearly an improvement in the accuracy of the estimated overlap with an order of magnitude, and the accuracy does not decrease significantly with an increasing number of qubits as unmitigated SWAP-Test does.

- 
- [S1] S. Endo, S. C. Benjamin, and Y. Li, *Phys. Rev. X* **8**, 031027 (2018).
- [S2] B. Koczor, *Phys. Rev. X* **11**, 031057 (2021).
- [S3] T. C. Developers, “Cirq: A python framework for creating, editing, and invoking quantum circuits,” <https://github.com/quantumlib/Cirq> (Accessed: 2023-10-12).
- [S4] S. V. Isakov, D. Kafri, O. Martin, C. V. Heidweiller, W. Mruzckiewicz, M. P. Harrigan, N. C. Rubin, R. Thomson, M. Broughton, K. Kissell, E. Peters, E. Gustafson, A. C. Y. Li, H. Lamm, G. Perdue, A. K. Ho, D. Strain, and S. Boixo, “Simulations of quantum circuits with approximate noise using qsim and cirq,” (2021), arXiv:2111.02396 .
- [S5] F. Arute, K. Arya, R. Babbush, D. Bacon, J. C. Bardin, R. Barends, R. Biswas, S. Boixo, F. G. S. L. Brandao, D. A. Buell, B. Burkett, Y. Chen, Z. Chen, B. Chiaro, R. Collins, W. Courtney, A. Dunsworth, E. Farhi, B. Foxen, A. Fowler, C. Gidney, M. Giustina, R. Graff, K. Guerin, S. Habegger, M. P. Harrigan, M. J. Hartmann, M. Ho, Alanand Hoffmann, T. Huang, T. S. Humble, S. V. Isakov, E. Jeffrey, Z. Jiang, D. Kafri, K. Kechedzhi, J. Kelly, P. V. Klimov, S. Knysh, A. Korotkov, F. Kostritsa, D. Landhuis, M. Lindmark, E. Lucero, D. Lyakh, J. R. Mandrà, Salvatoreand McClean, M. McEwen, A. Megrant, X. Mi, K. Michielsen, M. Mohseni, J. Mutus, O. Naaman, M. Neeley, C. Neill, M. Y. Niu, E. Ostby, A. Petukhov, J. C. Platt, C. Quintana, E. G. Rieffel, P. Roushan, N. C. Rubin, D. Sank, K. J. Satzinger, V. Smelyanskiy, K. J. Sung, M. D. Trevithick, A. Vainsencher, B. Villalonga, T. White, Z. J. Yao, P. Yeh, A. Zalcman, H. Neven, and J. M. Martinis, *Nature* **574**, 505 (2019).
- [S6] B. Nachman, M. Urbanek, W. A. de Jong, and C. W. Bauer, *Npj Quantum Inf.* **6**, 84 (2020).
- [S7] Q. Zhu, S. Cao, F. Chen, M.-C. Chen, X. Chen, T.-H. Chung, H. Deng, Y. Du, D. Fan, M. Gong, C. Guo, C. Guo, S. Guo, L. Han, L. Hong, H.-L. Huang, Y.-H. Huo, L. Li, N. Li, S. Li, Y. Li, F. Liang, C. Lin, J. Lin, H. Qian, D. Qiao, H. Rong, H. Su, L. Sun, L. Wang, S. Wang, D. Wu, Y. Wu, Y. Xu, K. Yan, W. Yang, Y. Yang, Y. Ye, J. Yin, C. Ying, J. Yu, C. Zha, C. Zhang, H. Zhang, K. Zhang, Y. Zhang, H. Zhao, Y. Zhao, L. Zhou, C.-Y. Lu, C.-Z. Peng, X. Zhu, and J.-W. Pan, *Sci. Bull.* **67**, 240 (2022).
- [S8] S. Bravyi, S. Sheldon, A. Kandala, D. C. Mckay, and J. M. Gambetta, *Phys. Rev. A* **103**, 042605 (2021).
- [S9] M. Fanizza, M. Rosati, M. Skotiniotis, J. Calsamiglia, and V. Giovannetti, *Phys. Rev. Lett.* **124**, 060503 (2020).
- [S10] J. C. Garcia-Escartin and P. Chamorro-Posada, *Phys. Rev. A* **87**, 052330 (2013).